MiniBooNE Technical Note # 103 Version 2

The GEANT4-based beam Monte Carlo for MiniBooNE

Michel Sorel

January 27, 2005

Abstract

We describe the GEANT4 beam Monte Carlo program `BooNEG4Beam`, discuss the validation of the code, and present predictions for the ν_μ, $\bar{\nu}_\mu$, ν_e, $\bar{\nu}_e$ fluxes at the MiniBooNE detector.

Contents

1 What's new in this tech-note version, and "warning" flags from code validation 3

2 Purpose of the Code 4
2.1 Main requirement: a flexible hadronic physics interface . . . 4
2.2 Additional requirements . . . 5

3 Code structure and functionality 6
3.1 GEANT4 class categories . . . 6
3.2 MiniBooNE-specific classes . . . 9
3.3 How to run the simulation (and optionally to develop the source code) . . . 13
3.3.1 How to run a `BooNEG4Beam` job on the MiniBooNE cluster . . . 14
3.3.2 For code development or remote `BooNEG4Beam` installation only . . . 14

4 Geometry and event generator 16
4.1 Geometry . . . 16
4.2 Event generator . . . 17

5 Properties of typical MiniBooNE neutrinos 19

6 Individual physics processes 22
6.1 The MiniBooNE physics list . . . 22
6.2 Inelastic interactions of primary protons in the target material . . . 22
6.3 Other inelastic processes . . . 28
6.4 Elastic processes . . . 31
6.5 Ionisation by charged hadrons . . . 32
6.6 Multiple Coulomb scattering . . . 34
6.7 Particle trajectories in horn magnetic field . . . 35
6.8 Particle decays . . . 36

7 Pion fluxes 42
7.1 `Model_B`: a brief description . . . 42
7.2 Pion fluxes after the horn . . . 43
7.3 Pion fluxes after the collimator . . . 44

8 Neutrino fluxes at the MiniBooNE detector 45
8.1 Comparison of `BooNEG4Beam`/`Model_B` neutrino fluxes at the detector . . . 45
8.2 Dec04 neutrino flux predictions from `BooNEG4Beam`/`BooBeamNT` . . . 47

9 Conclusions 51

10 Acknowledgments 52

1 What's new in this tech-note version, and "warning" flags from code validation

This is a second version of BooNE Technical Note # 103. Here are the changes compared to version 1, written in October 2003:

- this section;
- all of the description and plots now refer to the current version R1-10 of the simulation code `BooNEG4Beam`, while the version 1 of the tech note corresponded to release R1-4. Many things have changes, motivating this update. Roughly, this corresponds to changes between the WIN03 and the Dec04 flux predictions;
- new section on "Properties of typical MiniBooNE neutrinos";
- more quantitative checks on several physics processes.

In the code validation process described in the next pages, most checks yielded satisfactory results. Below, only the checks that were not as satisfactory are listed, in "order of appearance" in the tech-note:

- Section 6.2: secondary protons and neutrons produced in p-Be interactions are currently predicted with MARS15. The production of these particles is estimated to affect about 7% of the total muon neutrino flux. A small fraction of this 7% fraction of secondary protons and neutrons, the one with transverse momentum p_t greater than 1 GeV/c, are generated with p_t=1 GeV/c in `BooNEG4Beam`. This should have a negligible effect on the neutrino flux predictions;
- Section 6.3: the MiniBooNE-specific physics model for inelastic interactions of $K_p > 7.5$ GeV protons in Beryllium is pretty different from the GEANT4 model used for $K_p < 7.5$ GeV protons, and more "continuity" would be desirable;
- Section 6.4: the proton-Beryllium elastic cross-section used in the simulation for 8 GeV protons is about 25% smaller than the high-energy prediction from Ref. [11];
- not shown in this tech-note: the redecay program predicts a wrong muon neutrino energy distribution from muon decays. This is a very small effect on muon neutrino flux predictions, since most muon neutrinos are due to pion or Kaon decays;
- Section 7: `BooNEG4Beam` predicts more $p_\pi < 1.5$ GeV/c pions reaching the downstream face of the horn and the end of the collimator, compared to `Model_B`. Possibly due to $p \to p \to \pi^+$ events not simulated in `Model_B`;
- Section 8.1: while `BooNEG4Beam` and `Model_B` predict very similar overall muon neutrino flux normalizations at MiniBooNE, one finds that the `BooNEG4Beam` prediction is 12% lower than the `Model_B` one, restricting the comparison to the only class of muon neutrino events simulated by `Model_B`, that is $p \to \pi^+ \to \nu_\mu$ events. Moreover, for these events, the `BooNEG4Beam` neutrino energy distribution at MiniBooNE is 50-60 MeV (or 7%) lower than the `Model_B` one, and the typical π^+ angles at decay are larger in `BooNEG4Beam` than in `Model_B`. It is unlikely that this effect is due to ionization or multiple Coulomb scattering processes, which are not simulated by `Model_B`, and it is not clear what is the cause of this discrepancy.

2 Purpose of the Code

2.1 Main requirement: a flexible hadronic physics interface

The purpose of the MiniBooNE beam Monte Carlo is to predict the fluxes at the MiniBooNE detector for all relevant neutrino species (ν_μ, $\bar{\nu}_\mu$, ν_e, $\bar{\nu}_e$) as a function of neutrino energy, per proton on target and per unit area. The flux understanding is of primary importance for most MiniBooNE analyses, including for example neutrino cross-section meaurements, and $\nu_\mu \rightarrow \nu_e$ and $\nu_\mu \rightarrow \nu_{\not{\mu}}$ oscillation analyses.

As a consequence, a major effort is underway to refine the flux predictions by using (or planning to use) experimental information affecting these predictions, both from MiniBooNE data and from elsewhere:

1. compilation and reanalysis of existing pion and Kaon production data in proton-Beryllium interactions for proton beam momenta in the $\sim 10\ GeV/c$ range;
2. analysis of the BNL E910 data for $\pi^\pm,\ K^\pm,\ K^0$ production in $p + Be$ interactions at 6.0, 12.4, and 17.5 GeV/c proton beam momentum, on a thin Be target (5% λ_{inel});
3. analysis of the CERN HARP data for $\pi^\pm,\ K^\pm,\ K^0$ production in $p + Be$ interactions at 8.9 GeV/c beam momentum, on Be targets of various thicknesses (5%, 50%, 100% λ_{inel});
4. unfolding techniques to extract the neutrino fluxes from the observed rates in the MiniBooNE detector, assuming known neutrino cross-sections and no neutrino oscillations. For example, one proposed method is given in [1], and other methods are possible;
5. analysis of Little Muon Counters (LMC) data to constrain the ν_e flux in the detector due to $K^\pm$ decays.

It is important for MiniBooNE to have a beam Monte Carlo simulation program that makes use of the experimental information listed above, in order to get our best possible estimate for the neutrino fluxes as a function of energy, and to assign well-defined overall uncertainties (as well as neutrino energy bin-to-bin correlations) for the neutrino fluxes.

The same type of approach, partially relying on information external to that of the neutrino detector itself, has been used successfully by other experiments, for example by the K2K [2] and NOMAD [3] experiments.

A single code with a flexible hadronic physics model interface is appealing in this respect: the user may wish to tune meson production in $p + Be$ interactions to use for estimating the neutrino fluxes and their associated uncertainty, without changing any other aspects of the simulation. The motivation for having a flexible hadronic physics interface is that the flux uncertainty is dominated by the secondary meson production uncertainty, and we can expect the many other physics processes (energy loss, multiple scattering, reinteractions, particle decay routines, etc.) and MiniBooNE-specific design issues (target region and decay volume geometry, transport in horn magnetic field, energy threshold for particles tracking, ntuple output format, etc.) not to change as much in time as we refine our flux understanding. In order to fully describe meson production in p-Be interactions, both the inelastic interaction length of proton in Be, and the final state of

p-Be inelastic interactions (multiplicity of various secondaries, and their kinematic distributions), should be controlled by the user.

These goals can be accomplished in a variety of ways. Here we discuss one posible tool to implement these features, based on the MiniBooNE GEANT4 beam Monte Carlo, `BooNEG4Beam`. The generalization and abstraction of physics processes is a key issue in the design of Geant4 [4]. All physics processes are treated in the same manner from the tracking point of view. The GEANT4 approach enables the user to create a process (e.g. hadronic interactions in Beryllium) and assign it to a dynamic particle type (e.g. 8 GeV protons). This openness allows the creation of processes for novel, domain-specific or customised purposes by users (e.g. a "HARP" physics process). The custom-defined physics models are defined in the initialization phase, and no reweighting procedure at the tracking level is necessary to match the desired production cross-sections.

2.2 Additional requirements

Apart from the flexibility in selecting a hadronic physics model for particle production in proton-Beryllium interactions, specific requirements for the MiniBooNE beam simulation tools are:

beamline geometry: capability to change the geometry specifications of the simulation, for example switching from a 50m to a 25m long MiniBooNE decay region, to HARP production measurements geometries, or to K2K aluminum target geometry (for comparison);

event generator: capability to change all beam optics parameters describing the Booster primary proton beam incident on the MiniBooNE target;

horn magnetic field: capability to change the MiniBooNE horn magnetic field;

other inelastic processes: capability to change hadronic model describing the hadronic interactions of secondaries in all materials;

particle biasing techniques: capability to boost the statistics on certain neutrino types at the MiniBooNE detector (e.g. ν_e's from Kaons), and therefore reduce the statistical uncertainty associated with the Monte Carlo simulation, by "sampling" more frequently certain particle types;

output: capability to store particle information such as particle identity, initial and final momentum, initial and final position, final polarization, for the full chain of particles in the parentage history yielding neutrinos at MiniBooNE (*e.g.* for protons, pions, and neutrinos in $p \to \pi^+ \to \nu_\mu$ events), in a form suitable for other MiniBooNE software tools.

The above list is not meant to be complete, but rather represent some of the current user interface commands that the user can execute within the execution of a G4 beam Monte Carlo simulation, in addition to the built-in G4 user interface commands. The structure of the GEANT4 kernel and the MiniBooNE GEANT4 application `BooNEG4Beam`, together with their available user interface commands, are given in Section 3.

3 Code structure and functionality

3.1 GEANT4 class categories

Readers who are familiar with the GEANT3 code structure and functionality can skip this section.

From the "Introduction to GEANT4", [4]:

Geant4 is a free software package composed of tools which can be used to accurately simulate the passage of particles through matter. All aspects of the simulation process have been included in the toolkit:

- *the geometry of the system,*
- *the materials involved,*
- *the fundamental particles of interest,*
- *the generation of primary events,*
- *the tracking of particles through materials and electromagnetic fields,*
- *the physics processes governing particle interactions,*
- *the response of sensitive detector components,*
- *the generation of event data,*
- *the storage of events and tracks,*
- *the visualization of the detector and particle trajectories, and*
- *the capture and analysis of simulation data at different levels of detail and refinement.*

Users may construct stand-alone applications or applications built upon another object-oriented framework. In either case the toolkit will support them from the initial problem definition to the production of results and graphics for publication. To this end, the toolkit includes:

- *user interfaces,*
- *built-in steering routines, and*
- *command interpreters*

which operate at every level of the simulation.

At the heart of Geant4 is an abundant set of physics models to handle the interactions of particles with matter across a very wide energy range. Data and expertise have been drawn from many sources around the world and in this respect, Geant4 acts as a repository which incorporates a large part of all that is known about particle interactions.

Geant4 is written in C++ and exploits advanced software-engineering techniques and object-oriented technology to achieve transparency. For example, the way in which cross sections are

input or computed is separated from the way in which they are used or accessed. The user can overload both of these features. Similarly, the computation of the final state can be divided into alternative or complementary models, according to the energy range, the particle type, and the material. To build a specific application the user-physicist chooses from among these options and implements code in user action classes supplied by the toolkit. A serious problem with previous simulation codes was the difficulty of adding new or variant physics models; development was difficult due to the increased size, complexity and interdependency of the procedure-based code. In contrast, object-oriented methods help manage complexity and limit dependencies by defining a uniform interface and common organizational principles for all physics models. Within this framework the functionality of models can be more easily recognized and understood, and the creation and addition of new models is a well-defined procedure that entails little or no modification to the existing code.

From the "GEANT4 User's Guide - For Application Developers", [4]:

The class category diagram designed for Geant4 is shown in the figure below. Each class category is represented by a box in the figure, and a "uses" relation by a straight line. The circle at an end of a straight line means the class category which has this circle uses the other category. A class category is a "cluster of [C++] classes that are themselves cohesive, but are loosely coupled relative to other clusters".

The following is a brief summary of the role of each class category in Geant4.

1. *Run and Event*
   These are categories related to the generation of events, interfaces to event generators, and any secondary particles produced. Their roles are principally to provide particles to be tracked to the Tracking Management.

2. *Tracking and Track*
   These are categories related to propagating a particle by analyzing the factors limiting the step and applying the relevant physics processes. The important aspect of the design was that a generalized Geant4 physics process (or interaction) could perform actions, along a tracking step, either localized in space, or in time, or distributed in space and time (and all the possible combinations that could be built from these cases).

3. *Geometry, Magnetic Field and CAD-Interface*
   These three categories manage the geometrical definition of a detector (solid modeling and interactions with CAD systems) and the computation of distances to solids (also in a magnetic field). The Geant4 geometry solid modeler is based on the ISO STEP standard and it is fully compliant with it, in order to be able to exchange geometrical information with CAD systems. A key feature of the Geant4 geometry is that the volume definitions are independent of the solid representation. By this abstract interface for the G4 solids, the tracking component works identically for various representations. The treatment of the propagation in the presence of fields has been provided within specified accuracy. An OO design allows us to exchange different numerical algorithms and/or different fields (not only B-field), without affecting any other component of the toolkit

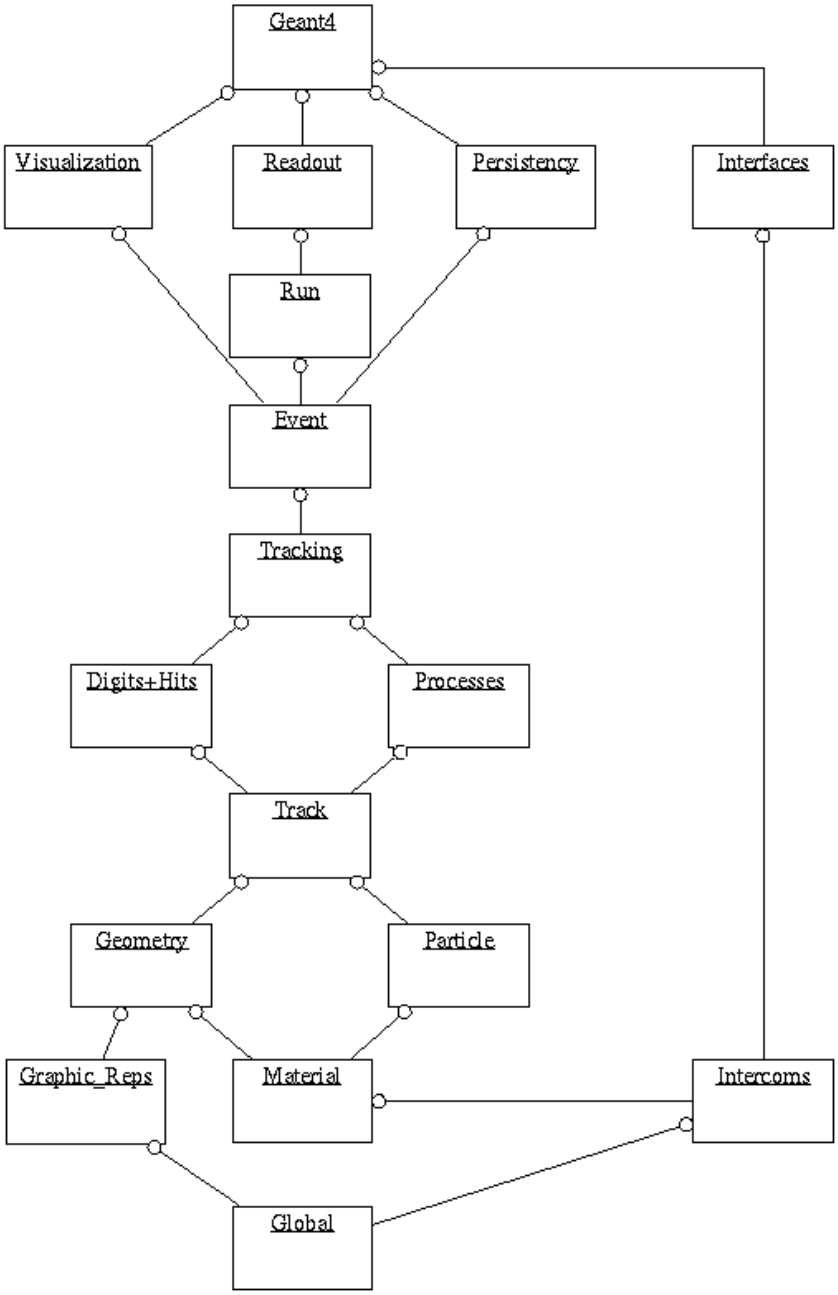

Figure 1: GEANT4 class categories. Eaich box represents a class category. The circle at the end of a straight line means that the class category which has this circle uses the other line-connected category.

4. *Particle Definition and Matter*
   These two categories manage the the definition of materials and particles.

5. *Physics*

This category manages all physics processes participating in the interactions of particles in matter. The abstract interface of physics processes allows multiple implementations of physics models per interaction or per channel. Models can be selected by energy range, particle type, material, etc. Data encapsulation and polymorphism make it possible to give transparent access to the cross sections (independently of the choice of reading from an ascii file, or of interpolating from a tabulated set, or of computing analytically from a formula). Electromagnetic and hadronic physics were handled in a uniform way in such a design, opening up the physics to the users.

6. *Hits and Digitization*
   These two categories manage the creation of hits and their use for the digitization phase. The basic design and implementation of the Hits and Digi had been realized, and also several prototypes, test cases and scenarios had been developed before the alpha-release. Volumes (not necessarily the ones used by the tracking) are aggregated in sensitive detectors, while hits collections represent the logical read out of the detector. Different ways of creating and managing hits collections had been delivered and tested, notably for both single hits and calorimetry hits types. In all cases, hits collections had been successfully stored into and retrieved from an Object Data Base Management System.

7. *Visualization*
   This manages the visualization of solids, trajectories and hits, and interacts with underlying graphical libraries (the Visualization class category). The basic and most frequently used graphics functionality had been implemented already by the alpha-release. The OO design of the visualization component allowed us to develop several drivers independently, such as for OpenGL and OpenInventor (for X11 and Windows), DAWN, Postscript (via DAWN) and VRML.

8. *Interfaces*
   This category handles the production of the graphical user interface (GUI) and the interactions with external software (OODBMS, reconstruction etc.)."

3.2 MiniBooNE-specific classes

The MiniBooNE GEANT4 application `BooNEG4Beam`, installed in *$BOONE_AFS/code13* and available in CVS, currently consists of:

1. `BooNEG4Beam.cc`, containing the main method of the application;

2. `jobOptions.in`, where user interface commands are specified (the user can change the name of this file);

3. utility scripts to set the G4 environment, to run G4 batch jobs, and to install the code;

4. libraries for each of the geometry specifications, in the `geometry/` subdirectory. Currently there are six geometry specifications, two for the MiniBooNE beamline (with and without a 25m absorber), three for MiniBooNE target geometries used in the HARP experiment at CERN, and one for K2K target geometry;

5. libraries for each of the physics models available for the description of various secondaries in inelastic interactions of primary protons in Beryllium, in the `physics/` subdirectory. Currently (release R1-10), depending on the particular secondary type, there are up to four physics models available;

6. 29 classes contained in the `src/` and `include/` subdirectories, representing the "meat" of the program.

A brief description of the 29 `BooNEG4Beam` classes follows. We start from some naming conventions:

1. filenames starting with `BooNE` refer to classes that have been specifically written or modified for the MiniBooNE beam Monte Carlo;

2. filenames starting with `ExN` refer to classes copied from GEANT4 novice examples classes of the current G4 distribution;

3. filenames ending in `Action` refer to user action classes. All objects of user action classes are registered with `G4RunManager`;

4. filenames ending in `Messenger` refer to `G4UImessenger` derived classes providing the MiniBooNE-specific interface commands available to the user in the `jobOptions.in` file. The availability of individual user interface commands, the ranges of parameters, the available candidates on individual command parameters may vary dynamically during the execution of the beam Monte Carlo job. All objects of messenger classes are instantiated in the respective user action class: for example, `BooNEPrimaryGeneratorActionMessenger` is instantiated in `BooNEPrimaryGeneratorAction`. For a complete list of all user interface commands available in `BooNEG4Beam`, the reader should consult the GEANT4 MiniBooNE web page, located at [5].

The MiniBooNE-specific classes can be subdivided according to the same class category given in the previous subsection. For more details on the software aspects of the simulation, the reader should consult the "Software Reference Manual" at [4], where many GEANT4 class header files can be browsed.

1. Run and Event

   i. `BooNERunAction`: inherits from the `G4UserRunAction` virtual class. Defines user actions at the run level of the simulation. The `BeginOfRunAction` and `EndOfRunAction` methods are used to communicate with the `BooNEOutput` interface class (see the "Interfaces" list later on in this section) to book and to write to file the ntuples with the results of the simulation for that particular run.

   ii. `BooNEEventAction`: inherits from the `G4UserEventAction` virtual class. Defines user actions at the event level of the simulation. The `RecordEndOfEvent` method is used to communicate with the `BooNEOutput` class to fill the ntuples information with selected trajectories.

   iii. `ExN03EventActionMessenger`: inherits from the `G4UImessenger` class and is instantiated in `BooNEEventAction`. Defines the event level user interface commands.

iv. `BooNEPrimaryGeneratorAction`: inherits from the `G4VUserPrimaryGeneratorAction` virtual class. Defines user actions at the event generator level of the simulation. The `GeneratePrimaries` method describes how initial particles are to be generated, typically 8 GeV protons.

v. `BooNEPrimaryGeneratorActionMessenger`: defines the interface commands available to the user at the event generator level. In particular, the parameters setting the primary beam optics description are implemented in this class.

2. Tracking and Track

vi. `BooNETrackingAction`: inherits from the `G4UserTrackingAction` virtual class. Defines user actions at the track level of the simulation. The `PreUserTrackingAction` and `PostUserTrackingAction` methods are used to copy track information at track's creation and destruction into the `BooNETrajectory` object (see `BooNETrajectory` description), for tracks that are relevant for the MiniBooNE neutrino fluxes predictions. Moreover, particle biasing techniques are implemented in this class, following the prescription first suggested by Byron Roe [6][1]. The motivation for particle biasing techniques in the MiniBooNE beam Monte Carlo is to allow the user to boost the statistics for intirnsic ν_e's in the beam while minimizing the impact on the CPU time of the simulation.

vii. `BooNETrackingActionMessenger`: defines the user interface commands available at track level. In particular, the user interface commands to select particle biasing techniques are defined in this class.

viii. `BooNETrackInformation`: inherits from the `G4VUserTrackInformation` virtual class and is instantiated in `BooNETrackingAction`. This class specifies additional track information, such as the GEANT3 particle encoding scheme and the MiniBooNE neutrino encoding scheme.

ix. `BooNETrajectory`: inherits from the `G4VTrajectory` virtual class and is instantiated in `BooNETrackingAction`. This class represents the trajectory of a tracked particle, and contains the list of trajectory points which compose the trajectory, static (e.g. charge, mass, etc.) as well as dynamic (e.g. momentum, position, etc.) information of the track, and the identifier of its parent trajectory. Most of this information is taken from the `G4Ttrack` class, as well as from `BooNETrackInformation`. This class is needed for two reasons: first, `G4Track` objects are transient objects, and do not exist in memory anymore by the time the end of the event is reached, when the ntuple is being filled; second, the `BooNETrajectory` class makes it possible to select tracks based on the parent (or previous ancestor) track information. `BooNETrajectory` makes tracks persistent until the end of an event, and stores all the information needed by the beam Monte Carlo.

x. `BooNESteppingAction`: inherits from the `G4UserSteppingAction` virtual class. Defines user actions at the step level of the simulation. In particular, tracks which are not relevant for the MiniBooNE neutrino fluxes predictions are killed, and optional ntuples with extra track information can be filled by this class, for debugging purposes.

[1] In release R1-10, particle biasing has been, temporarily, turned off, because of memory leaks when running with the GEANT4 v6.6.p02 distribution. This useful biasing technique will re-enabled as soon as the memory problems will be resolved.

xi. `BooNESteppingActionMessenger`: defines the user interface commands available at step level. In particular, the user interface commands to select perfect focusing of secondaries is set in this class.

3. Geometry, Magnetic Field and CAD-Interface

   xii. `BooNEGeometryConstruction`: inherits from the `G4VUserDetectorConstruction` class and is registered with `G4RunManager`. Defines the geometry of the simulation: volumes, volume attributes such as the horn magnetic field, and materials. With the exception of the magnetic field, all "geometry" specifications are automatically converted from the corresponding GEANT3.21 geometries, using the call list interpreter `G4BuildGeom.cc` of the `G3toG4` facility.

   xiii. `BooNEGeometryConstructionMessenger`: defines the user interface command specifying the geometry call list filename.

   xiv. `BooNELocalField`: inherits from the `G4MagneticField` class and is instantiated in `BooNEGeometryConstruction`. For the MiniBooNE geometry files, defines a local, non-uniform magnetic field within the horn volume (via the `GetFieldValue` method), and defines various options for integrating the equation of motion of the particle in that field.

   xv. `BooNELocalFieldMessenger`: defines the user interface command specifying the horn electric current.

4. Particle Definition and Matter: none

5. Physics

   xvi. `BooNEPhysicsList`: inherits from the `G4VModularPhysics` virtual class and is instantiated in the `main` method of the simulation. This is the top-level class for constructing particles and physics processes. The classes describing the general, electromagnetic, muon, hadron, and ion physics are registered to the process manager in `BooNEPhysicsList`.

   xvii. `BooNEHadronPhysics`: inherits from the `G4VPhysicsConstructor` virtual class and is instantiated in `BooNEPhysicsList`. Constructs all mesons, baryons, resonances and quarks, and physics processes specific to these particles.

   xviii. `BooNEHadronPhysicsMessenger`: defines the user interface commands specifying the physics model to be used for hadronic interactions other than the hadronic interaction of primary protons in Beryllium (separately described by `BooNEpBeInteraction` and `BooNEpBeCrossSection`).

   xix. `BooNEpBeInteraction`: inherits from the `G4HadronicInteraction` class and is instantiated in `BooNEHadronPhysics`. Defines secondary particle production (particle types, multiplicities, momenta) for inelastic interactions of primary protons in Beryllium, that is fully describe the final state of inelastic p-Be interactions.

   xx. `BooNEpBeInteractionMessenger`: defines the user interface commands specifying the physics model to be used for inelastic interactions of primary protons in Beryllium.

   xxi. `BooNEpBeCrossSection:` inherits from the `G4VCrossSectionDataSet` and is instantiated in `BooNEHadronPhysics`. Defines the proton-Beryllium inelastic cross-section, and therefore allows the user to control how often, and at which average position within the target, the `BooNEpBeInteraction` class is called.

xxii. `ExN04EMPhysics`: inherits from the `G4VPhysicsConstructor` virtual class and is instantiated in `BooNEPhysicsList`. Constructs photons, electrons and neutrinos, and physics processes specific to these particles.

xxiii. `ExN04GeneralPhysics`: inherits from the `G4VPhysicsConstructor` virtual class and is instantiated in `BooNEPhysicsList`. Defines particle decays.

xxiv. `ExN04IonPhysics`: inherits from the `G4VPhysicsConstructor` virtual class and is instantiated in `BooNEPhysicsList`. Defines nuclei and light ions (e.g.deuterons, etc.), and physics processes specific to these particles.

xxv. `ExN04MuonPhysics`: inherits from the `G4VPhysicsConstructor` virtual class and is instantiated in `BooNEPhysicsList`. Defines muons and tau leptons, and physics processes specific to these particles.

6. Hits and Digitization: none

7. Visualization

xxvi. `ExN02VisManager`: inherits from the `G4VisManager` virtual class and is instantiated in the `main` method of the simulation. Defines the graphics systems to be used for geometry and tracks visualization via the `RegisterGraphicsSystems` method. Exploits C-pre-processor variables (e.g `G4VIS_USE_DAWN`, etc.) which are set by the GNUmakefiles if the environment variables of the same name are set. Several graphics systems are registered and available in `BooNEG4Beam`; the only one tested (and working very nicely) is `VRML2FILE`, creating GEANT4 scenes in VRML formats (version 2). Several VRML browsers for Linux can be downloaded for free (e.g. `http://www.sim.no`).

8. Interfaces

xxvii. `BooNEOutput`: this class is instantiated in the `main` method of the simulation. This class stores track and parent track information for selected tracks into HBOOK ntuples. In addition, the muon polarization vector in its rest frame is calculated, as done in the GEANT3 MiniBooNE beam Monte Carlo by Geoff Mills. `BooNEOutput` uses `cfortran` to bridge the FORTRAN HBOOK and CERNLIB codes to the GEANT4 C++ code. This class is based on a class originally written by Bill Seligman for the G4 simulation of the ATLAS electromagnetic barrel calorimeter.

xxviii. `BooNEOutputMessenger`: defines the user interface commands specifying the options for the simulation output: which ntuples should be written, and with which kinematic selection on tracks and parent tracks.

xxix. `BooNENtupleHandler`: this class defines methods for operations on HBOOK ntuples, such as ntuple definition, filling, writing to file.

3.3 How to run the simulation (and optionally to develop the source code)

The information below contains a brief, practical explanations on how to run the simulation, and optionally how to develop the source code. This Section is taken from the `BooNEG4Beam README` file.

3.3.1 How to run a `BooNEG4Beam` job on the MiniBooNE cluster

- The last stable version of the BooNEG4Beam executable (release R1-10) is now in your path, so you don't need to copy the source code locally and build it anymore
- Just copy a template jobOptions file and the setup.env file, either:
  1. `cp $G4WORKDIR/jobOptions.in`, `cp $G4WORKDIR/setup.env`, or:
  2. `cvs export -r R1-10 BooNEG4Beam/jobOptions.in`,
     `cvs export -r R1-10 BooNEG4Beam/setup.env`
- Type: `source setup.env`. This will setup geant4 and several environment variables The beam MC executable is located in the $G4WORKDIR directory
- Modify the jobOptions.in file as you wish. You can use the commands and values listed in: `http://www-boone.fnal.gov/software_and_analysis/beam_group/software/links/geant4/doc/_.html`
- Run from a shell with the G4 environment already set: `BooNEG4Beam jobOptions.in`
- Run on CONDOR: `boone-jobsub -M BooNEG4Beam_wrapper.csh` This wrapper sets the G4 environment picked up by CONDOR, and executes `BooNEG4Beam`
- The ntuples format is explained in: `http://www-boone.fnal.gov/software_and_analysis/beam_group/software/links/geant4/doc/ntuplesoutput.html`

3.3.2 For code development or remote `BooNEG4Beam` installation only

Follow the steps below to get the source code, setup the GEANT4 environment, and compile the source code.

- Get the source code
  1. If you already have an existing version of BooNEG4Beam: `cd` to the existing BooNEG4Beam directory, type: `cvs update`
  2. If you don't have an existing version of BooNEG4Beam, type `cvs checkout BooNEG4Beam` or, for remote installation, `cvs export -r R1-10 BooNEG4Beam`
- Setup the GEANT4 environment
  1. `cd BooNEG4Beam`
  2. Modify the G4WORKDIR environment variable, so that it points to a local directory of yours, and not to the MiniBooNE one (default case), for example: `setenv G4WORKDIR $PWD`
  3. `source setup.env`
  4. For remote installation, you might have to change the `setup geant4` line, depending on how G4 is set up on your machine

- Compile the code
  Type `gmake`. Depending on your compilation options, you might get warnings, mostly due to the cfortran package, but hopefully no errors. As is, the code works on the Linux platform only.

- Run the code
  Follow the steps listed above. To run on CONDOR, the user needs to add the line `setenv G4WORKDIR $PWD` before the line `source setup.env` in `BooNEG4Beam_wrapper.csh`, in order to point to the local `BooNEG4Beam` version.

4 Geometry and event generator

In this Section we discuss the concrete implementation in `BooNEG4Beam` of two mandatory G4 user action classes: the geometry construction and primary generator classes.

4.1 Geometry

As far as geometry and materials definitions are concerned, `BooNEG4Beam` reuses the work done for the GEANT3.21 beam Monte Carlo, `BooBeamMC`, by automatically converting G3 geometries and materials into G4 via the `G3toG4` facility in G4. Therefore, no coding of geometry specifications in G4 has been necessary. The automatic conversion is done in three steps:

G3→RZ : run the G3 beam Monte Carlo in interactive mode (i.e. run the `gxint` executable), to convert the MiniBooNE geometry data structure specified in the G3 cardfile into an RZ file;

RZ→ASCII : once the RZ file is available, it can be converted into an ASCII call list file by running the `rztog4` GEANT4 utility. This ASCII file contains the instructions on how to build the geometry. Examples of such files, which are human-readable and reflect the G3 syntax, can be found in the `geometry/` subdirectory of `BooNEG4Beam`. The source code of `rztog4` is FORTRAN;

ASCII→G4 : the call list interpreter `G4BuildGeom.cc`, called in `BooNEGeometryConstruction.cc` and defined in `$G4INSTALL/source/g3tog4`, read the instructions in ASCII format and builds the geometry in the G4 code.

For consistency, all geometry specifications in `BooNEG4Beam` are given in the form of an ASCII call list file. In the `geometry/` subdirectory, there are currently six possible choices of geometries and materials specifications:

1. `BooNE_50m.geom`: MiniBooNE geometry with a 50 m long decay region;
2. `BooNE_25m.geom`: MiniBooNE geometry with a 25 m long decay region;
3. `HarpTarget_5.geom`: Be target and support structure for the 5% λ_{inel} Be target used during the data-taking in the HARP detector in summer 2002 (λ_{inel} refers to the inelastic interaction length);
4. `HarpTarget_50.geom`: Be target and support structure for the 50% λ_{inel} Be target used in HARP. This target is made of two out of the seven 25% λ_{inel} Be slugs currently used in the MiniBooNE beamline;
5. `HarpTarget_100.geom`: Be target and support structure for the 100% λ_{inel} Be target used in HARP. This target is made of four out of the seven 25% λ_{inel} Be slugs currently used in the MiniBooNE beamline;
6. `K2K_Target.geom`: K2K Al target.

For the three HARP targets, the geometry specifications were already given in ASCII format, and the G3→RZ→ASCII conversion was not necessary.

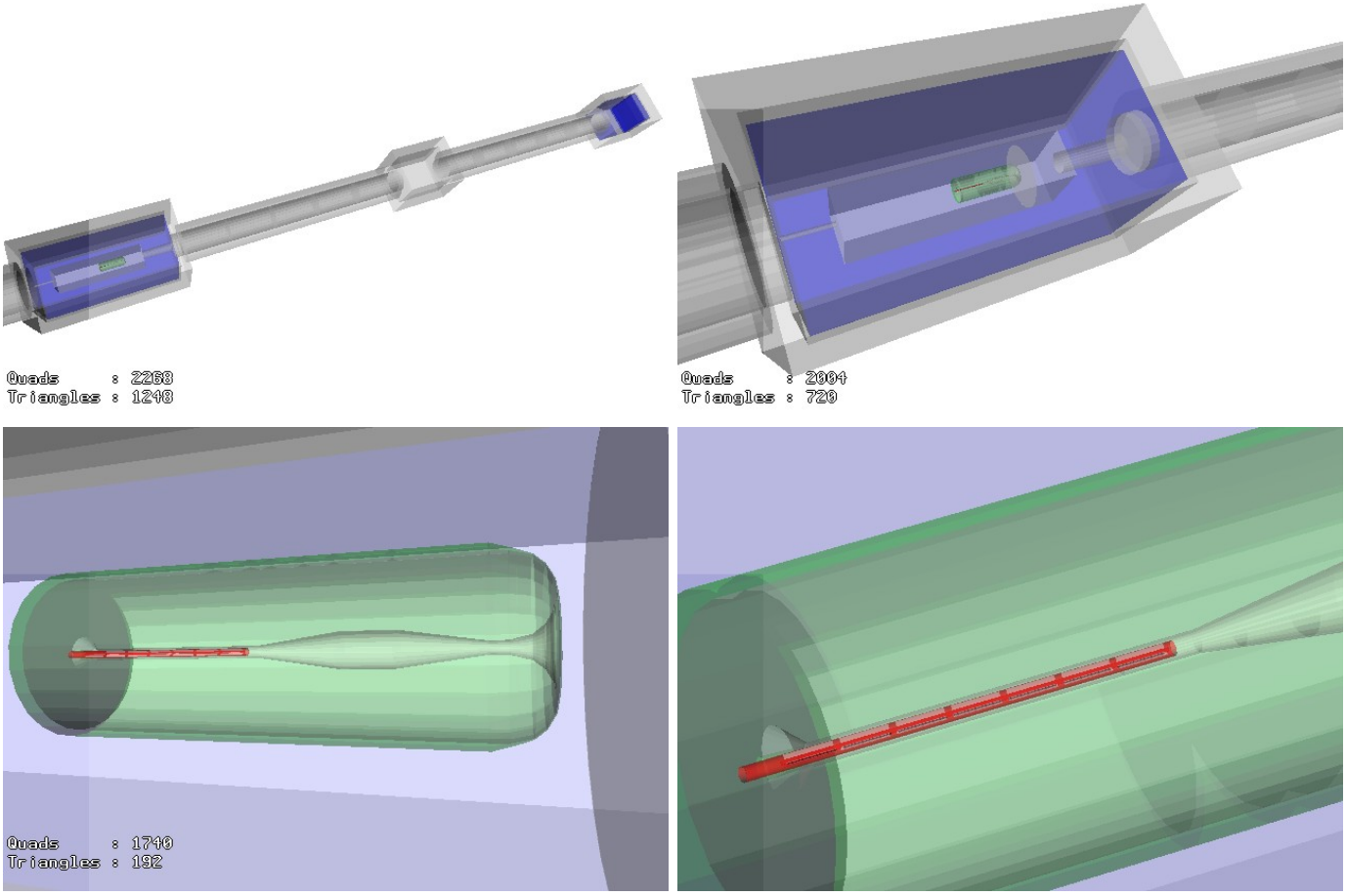

Figure 2: Snapshots of the MiniBooNE geometry implemented in the beam Monte Carlo. Pictures refer to the 50 m long decay region configuration. From the top left picture, in clock-wise order: picture of the entire 50 m decay region; detail of the target pile region; detail of the horn; detail of the target.

In Fig.2, four images of the `BooNE_50m.geom` geometry are shown. The images show the entire decay region, and details of the target pile region, horn, and target. The volumes shown in red are made with Beryllium, the regions shown in blue with iron. The other two relevant materials are concrete fro the decay region walls and for the collimator downstream of the horn, and Aluminum for the MiniBooNE horn. These images are produced by running `BooNEG4Beam` with the `VRML2FILE` graphics system, and then creating snapshots of the graphics scene from the `vrmlview` VRML viewer. The geometry is identical to the G3 one.

4.2 Event generator

The event generator in `BooNEG4Beam` is very simple: all that is needed is to construct one primary proton per event with 8 GeV kinetic energy, directed towards the Be target. To account for the fact that the beam optics is not perfect, some smearing in the initial transverse position (x, y) and

Parameter	x_0	σ_x	y_0	σ_y	z_0	$\theta_{x,0}$	$\sigma_{\theta,x}$	$\theta_{y,0}$	$\sigma_{\theta,y}$
Value	0	1.51 mm	0	0.75 mm	-10 mm	0	0.66 mrad	0	0.40 mrad

Table 1: Central values for the beam optics parameters used in the Dec04 baseline. See text for definitions. The MiniBooNE Be target is located at: $3.5 < z\ (cm) < 74.6$, $\sqrt{x^2+y^2} < 4.76$ cm.

angular divergence (θ_x, θ_y) of the beam can be introduced. Also, the user can change the mean (x_0, y_0) positions and the mean $(\theta_{x,0}, \theta_{y,0})$ directions of the primary beam. The user also controls the longitudinal position z_0 for the primary proton at birth; all beam optics parameters refer to this position. The position and angular smearing are described by gaussian distributions. More specifically, the initial position and momentum of the generated primary proton are [2]:

$$\begin{cases} x = x_0 + \sigma_x \texttt{ran1} \\ y = y_0 + \sigma_y \texttt{ran2} \\ z = z_0 \\ p_x = \sqrt{E_p^2 - m_p^2}(\theta_{x,0} + \sigma_{\theta_x} \texttt{ran3}) \\ p_y = \sqrt{E_p^2 - m_p^2}(\theta_{y,0} + \sigma_{\theta_y} \texttt{ran4}) \\ p_z = \sqrt{E_p^2 - m_p^2 - p_x^2 - p_y^2} \end{cases} \tag{1}$$

where `ran1`, `ran2`, `ran3`, `ran4` are four random numbers drawn from a gaussian distribution centered at zero and with an RMS of one, $E_p = K_p + m_p$, where K_p=8 GeV and m_p is the proton mass, and the parameters x_0, σ_x, y_0, σ_y, z_0, $\theta_{x,0}$, σ_{θ_x}, $\theta_{y,0}$, σ_{θ_y} are nine parameters that can be set by the user in the `jobOptions.in` file. The default values used in the Dec04 baseline are given in Tab. 1.

The values of the beam optics parameters listed in Tab. 1 were provided by Jocelyn Monroe and Al Russell, and are the results of beam simulations extrapolated to the front face of the target. These simulations are in good agreement with measurements. Currently, no correlations between beam optics parameters are implemented in `BooNEG4Beam`, therefore the primary beam defocuses over distance if σ_x and/or σ_y are nozero. It is estimated that this choice of beam optics parameters yields a 99.8% targeting efficiency [3].

[2] The small-angle appropximation is assumed throughout the simulation of primary beam parameters.

[3] This is about a 10% increase in targeting efficiency compared to the Feb04 parameters, translating into a 15-20% increase in neutrino flux predictions from beam optics changes alone, once inelastic interactions of protons in Beryllium and other effects are taken into account.

5 Properties of typical MiniBooNE neutrinos

In Section 6, we will discuss several physics processes of relevance for MiniBooNE flux predictions. As an introduction to Section 6, we first discuss some properties of typical events yielding neutrinos at the MiniBooNE detector, as predicted by the `BooNEG4Beam` simulation. This Section gives some qualitative idea of what "relevant" means.

Table 2 shows the predicted neutrino flavor composition of the MiniBooNE neutrino flux in neutrino running. The flux is dominated by muon neutrinos, comprising 92.7% of the total neutrino flux, with a 6.6% flux contribution from muon antineutrinos. Electron neutrinos comprise about 0.6% of the total neutrino flux.

Table 3 shows the most likely "neutrino history" for neutrinos reaching MiniBooNE, divided per neutrino flavor. The muon neutrino flux is mostly (86.1%) due to the decay of positive pions, from pions that are in turn created directly by inelastic interactions of primary protons.

Neutrino Flavor	Flux fraction (%)
ν_μ	92.7
$\bar{\nu}_\mu$	6.6
ν_e	0.6
$\bar{\nu}_e$	0.1

Table 2: Neutrino flavor composition of the MiniBooNE neutrino flux in neutrino running, as predicted by `BooNEG4Beam`.

Neutrino Flavor	Process	Flux fraction per flavor (%)
ν_μ	$p \to \pi^+ \to \nu_\mu$	86.1
	$p \to p \to \pi^+ \to \nu_\mu$	7.3
	$p \to K^+ \to \nu_\mu$	2.8
	$p \to n \to \pi^+ \to \nu_\mu$	1.9
	Other	1.9
$\bar{\nu}_\mu$	$p \to \pi^- \to \bar{\nu}_\mu$	55.0
	$p \to p \to \pi^- \to \bar{\nu}_\mu$	16.6
	$p \to n \to \pi^- \to \bar{\nu}_\mu$	12.0
	Other	16.4
ν_e	$p \to \pi^+ \to \mu^+ \to \nu_e$	47.6
	$p \to K^+ \to \nu_e$	32.7
	$p \to K^0_L \to \nu_e$	7.2
	$p \to p \to \pi^+ \to \mu^+ \to \nu_e$	5.0
	Other	7.5
$\bar{\nu}_e$	$p \to K^0_L \to \bar{\nu}_e$	65.5
$\bar{\nu}_e$	$p \to \pi^- \to \mu^- \to \bar{\nu}_e$	9.8
	Other	24.7

Table 3: Most likely history for neutrinos reaching the MiniBooNE detector, as simulated by the beam Monte Carlo, for each neutrino flavor. The arrows indicate either an inelastic interaction, or a decay.

Quantity	Description	Value
$\langle p_{\pi+,in} \rangle$	Initial π^+ momentum	2.17 GeV/c
$\langle \vartheta_{\pi+,in} \rangle$	Initial π^+ angle	106 mrad
$\langle l_{\pi+,B} \rangle$	π^+ path in horn field	82.1 cm
$\langle B_{\pi+} \rangle$	Horn field along π^+ trajectory	0.71 Tesla
$\langle p_{\pi+,fin} \rangle$	Final π^+ momentum	2.08 GeV/c
$\langle \vartheta_{\pi+,fin} \rangle$	Final π^+ angle	30 mrad
$\langle E_\nu \rangle$	Neutrino energy	0.762 GeV

Table 4: Average properties for $p \to \pi^+ \to \nu_\mu$ processes giving muon neutrinos at MiniBooNE, as simulated by the beam Monte Carlo. The properties in this Table illustrate pion production, focusing, and decay kinematics characteristics.

The contribution of muon neutrinos from pions created by secondary protons and neutrons is also non-negligible, as is non-negligible the contribution of muon neutrinos from charged Kaon decays. Electron neutrinos are dominated by the decays of muons produced by positive pions, which are in turn directly produced in inelastic interactions of primary protons (48.0% of the total electron neutrino flux). Contributions to the electron neutrino flux from charged and neutral Kaon decays, and from other muon decay chains, are also significant.

The remaining two tables focus on muon neutrinos, and in particular on the $p \to \pi^+ \to \nu_\mu$ events that mainly contribute to the total muon neutrino flux. Table 4 lists average properties concerning pion production, focusing, and pion decay kinematics. Pions yielding muon neutrinos at MiniBooNE are produced in the Beryllium target with an average momentum and angle of $\sim$ 2.2 GeV/c and $\sim$ 100 mrad, respectively. Pions loose some energy crossing various materials, and are focused by a $\sim$ 1 Tesla horn magnetic field over distances of the order of $\sim$ 1 meter, as well as by the collimator system, resulting in average pion angles at decay of about 30 mrad. Neutrinos reaching the MiniBooNE detector are produced forward in the pion centerof-mass frame, resulting in typical neutrino energies that are a little less than the maximum neutrino energy of $E_\nu = (m_\pi^2 - m_\mu^2)E_\pi/m_\pi^2$, where m_π and m_μ are π^+ and μ^+ masses, respectively, and E_π is the total π^+ energy at decay.

Table 5 shows other properties for $p \to \pi^+ \to \nu_\mu$ events yielding muon neutrinos at MiniBooNE, related to beamline geometry, energy loss, and pion decay characteristics. Primary protons travel about 22 cm on average in the Be target before producing positive pions [4], loosing about 50 MeV of energy. The pions that are produced by protons interact via several physics processes (see next Section), and loose a small fraction of their energy, in Beryllium, Aluminum, and iron before decaying into neutrinos.

[4]Note that this is significantly less than the inelastic interaction length, see next Section.

Particle	Material	$\langle \Delta E \rangle$ (MeV)	$\langle l \rangle$ (cm)
p	Beryllium	56.3	22.3
π^+	Aluminum	22.3	5.9
π^+	Beryllium	21.5	8.5
π^+	Iron	11.3	1.1
π^+	Concrete	6.5	2.9
π^+	Air	2.9	1900

Table 5: Average properties for $p \to \pi^+ \to \nu_\mu$ processes giving muon neutrinos at MiniBooNE, as simulated by the beam Monte Carlo. The properties in this Table illustrate beamline geometry, energy loss, and pion decay characteristics.

6 Individual physics processes

6.1 The MiniBooNE physics list

As discussed in Section 3, the classes `BooNEPhysicsList`, `BooNEHadronPhysics`, `ExN04EMPhysics`, `ExN04GeneralPhysics`, `ExN04IonPhysics`, and `ExN04MuonPhysics` register all physics processes to be used in the G4 simulation. Physics processes are chosen by instantiating a certain physics model describing that process; different particle types have in general a different list of physics processes registered and/or different models describing a given process. Moreover, for a given particle type, different models can be selected according to the kinetic energy of the particle and the target material that the particle is traversing. In addition to physics models describing the final state for various processes, cross-section datasets are instantiated in these classes, fixing how often these processes are called. The applicability range of cross-section models follows the same philosophy as for final state models, and different cross-section models can be registered depending on the projectile type, projectile energy, and target material.

In this section, we validate some of the physics processes of greatest relevance to MiniBooNE by adopting the following simple philosophy: we turn off all of the physics processes in `BooNEG4Beam`, except the one we are interested in, and we analyse the outcomes of the simulation. We repeat this method for a number of conditions: different processes, particle types, momenta, materials.

In `BooNEG4Beam`, only one physics model does not belong to the fairly extensive list of choices available among the built-in G4 models (for more details on the built-in G4 physics models, the reader should consult the "Physics Reference Manual" available at [4]). This physics model is a custom-defined model describing inelastic collisions of protons with a kinetic energy $K_{p,0} - 500$ MeV $< K_p < K_{p,0} + 10$ MeV, where $K_{p,0}$ is the primary beam kinetic energy, in the target material only, as specified by the target volume name `TARG`. For the simulation of the MiniBooNE beam, $K_{p,0} = 8$ GeV, and the target material is Beryllium. The final state description part is implemented in `BooNEpBeInteraction`; the cross-section part is implemented in `BooNEpbeCrossSection`. We start this Section by discussing this particular model, then we discuss the other physics processes affecting the MiniBooNE neutrino flux.

6.2 Inelastic interactions of primary protons in the target material

The inelastic interaction cross-section of primary protons in the target material is implemented by the custom-defined `BooNEpBeCrossSection` class. There are three possible cross-section models:

`GFLUKA` : the total inelastic cross-section is computed via the command `GPLMAT` in a GEANT3.21 simulation, where the mechanism name is set to 'HADF'. `BooNEG4Beam` currently has three tables of GFLUKA hadronic cross-sections between 1 and 20 GeV/c proton projectile momentum, for Beryllium, Aluminum, and iron target materials. For 8.9 GeV/c protons on Beryllium, the total GFLUKA inelastic cross-section is 199.7 mb.

`MARS` : the total inelastic cross-section is computed via a MARS15 simulation, `MARSinelxsec`. As for GFLUKA, `BooNEG4Beam` has inelastic cross-section tables for Beryllium, Aluminum, and iron target materials, and for primary proton momenta between 1 and 20 GeV/c. For 8.9 GeV/c protons on Beryllium, the total MARS inelastic cross-section is 220.5 mb.

`BooNE` : the total inelastic cross-section is set by the user via the command `/boone/physics/pBeInelasticXSecUser`. This is the default cross-section model used in the Dec04 baseline, with an inelastic cross-section value of $\sigma_{inel} = 189.3$ mb. This value was extracted from BNL E910 data, and corresponds to an inelastic interaction length of $\lambda_{inel} = A/(\rho N_{Av}\sigma_{inel})$=42.8 cm, where $A = 9.01\ g/mol$ is the atomic weight of Beryllium, $N_{Av} = 6.022 \cdot 10^{23}\ mol^{-1}$ is Avogadro's number, and $\rho = 1.848\ g/cm^3$ is the Beryllium density.

At MiniBooNE, for 7.5 GeV $< K_p <$ 8.01 GeV protons in Beryllium, the final state of all inelastic interactions is described by the `BooNEpBeInteraction` class. This is the physics process whose uncertainties affect the most the neutrino flux in MiniBooNE, and the one about which we seek to gather as much information as possible from past particle production experiments, BNL E910, and HARP.

What `BooNEpBeInteraction` does can be described by the following steps:

1. given one of the physics models supported by `BooNEpBeInteraction`, the average multiplicity per inelastic collision for various secondary particles is computed. There are currently seven types of particles produced: secondary protons, neutrons, π^+, π^-, K^+, K^-, K^0_L; therefore, seven multiplicities are computed. This is done once for the entire G4 simulation. The average multiplicity per inelastic collision is computed by dividing the inclusive production cross-section for each given secondary particle type by the total proton-Beryllium inelastic cross-section, σ_{inel}, discussed above. The inclusive production cross-sections are given in the form of tables of double-differential cross-sections, as a function of longitudinal (p_z) and transverse (p_t) momentum for the secondary particle, with respect to the initial projectile direction. The numbers in the cross-section tables are given in units of $mb/(GeV/c)^2$. The numerator in the above ratio defining the average multiplicity per inelastic interaction is given by summing the double-differential cross-section over all (p_z, p_t) bins;

2. when `BooNEpBerInteraction` is called by the G4 process manager, the number and composition of final state particles is selected by drawing seven multiplicity numbers, one for each of the secondary particle types, from Poisson distributions with the average multiplicities calculated [5]. The corresponding particles are then created as daughter particles of the projectile particle;

3. for each of the final state particles created, their 3-momentum is assigned according to the double-differential cross-section tables. This is done by applying a simple accept/reject method to the 2-dimensional (p_z, p_t) probability distribution function, obtained from a linear interpolation of the disctretized $\Delta^2\sigma/\Delta p_z \Delta p_t$ cross-section table. The cross-section table contains 50×100 $p_z \times p_t$ bins over the ranges $(0 < p_z < 10$ GeV/c$, 0 < p_t < 1$ GeV);

4. the original incidient particle as well as the struck Be nucleus are deleted from the particle stack;

5. if requested, ntuple 102 with the secondary particles information is filled. This is optional, and present for debugging purposes only. This ntuple being filled at the process level of the

[5] The specific functional form of the distribution is not important, here: any distribution with the same average multiplicity as the Poisson one would serve the purpose equally well.

Physics Model	Secondary particle						
	p	n	π^+	π^-	K^+	K^-	K^0_L
GFLUKA	√	√	√	√	√	√	√
MARS	√	√	√	√	√	√	√
ZGS			√	√			
SWPar			√	√	√		√

Table 6: Production models available for the various secondaries in p-Be inelastic interaction. See text for details.

simulation, while the default ntuple 101 is being filled at the event level (see Fig.1 to see the relation between event and processes).

We note here that is no longer necessary to rotate the momentum vector of the secondary particles according to the initial projectile direciton, since this rotation is now taken care of internally by the G4 code.

The `BooNEG4Beam` user can currently choose among up to four production models, depending on the secondary particle type: `GFLUKA`, `MARS`, `ZGS`, `SWPar`. The production model for a given secondary can now be chosen independently of the production models chosen for the other secondaries, so that several physics model combinations are possible. The assumptions for these models are explained below, and are summarized in Tab.6:

`GFLUKA` : p, n, $\pi^\pm$, $K^\pm$, K^0_L production is described according to the cross-section tables contained in the file `GFLUKAData.hh` in the `physics/` subdirectory. These seven cross-section tables were all extracted from an *ad hoc* GEANT3.21 simulation of 25 million 8 GeV protons traversing a thin block of Be material, choosing the FLUKA physics option in GEANT3.21.

`MARS` : p, n, $\pi^\pm$, $K^\pm$ production is described according to the cross-section tables contained in the file `MARSData.hh` in the `physics/` subdirectory. These six cross-section tables were all extracted from an *ad hoc* MARS15 simulation of 100 million 8 GeV protons in Beryllium, using the `MARSinelxsec` code in CVS. A different approach is used for K^0_L, given the fact that MARS does not store K^0_L particles. In this case, the K^0_L yield in any (p_z, p_t) bin is constructed from the MARS K^+ yield, times the GFLUKA K^0_L/K^+ yield ratio:

$$\frac{d^2N_{K_L,MARS}}{dp_z dp_t} \equiv \frac{d^2N_{K^+,MARS}}{dp_z dp_t} \cdot \left(\frac{d^2N_{K_L,GFLUKA}}{dp_z dp_t} / \frac{d^2N_{K^+,GFLUKA}}{dp_z dp_t}\right) \tag{2}$$

`ZGS` : $\pi^\pm$ production is described according to the Sanford-Wang parametrization of $\pi^\pm$ production data from Argonne's ZGS data, described in [8]. The Sanford-Wang parametrization for the $\pi^\pm$ inclusive double-differential cross-section is defined by sixteen parameters, $c^\pm_1, \ldots, c^\pm_8$, eight for π^+ production, eight for π^- production:

$$\frac{d^2\sigma(p + Be \to \pi^\pm + X)}{dp d\Omega} = c^\pm_{\pi,1} p^{c^\pm_{\pi,2}} \left(1 - \frac{p}{p_{beam} - 1}\right) \exp\left[-c^\pm_{\pi,3} \frac{p^{c^\pm_{\pi,4}}}{p_{beam}^{c^\pm_{\pi,5}}} - c^\pm_{\pi,6} \vartheta \left(p - c^\pm_{\pi,7} p_{beam} \cos^{c^\pm_{\pi,8}} \vartheta\right)\right] \tag{3}$$

Secondary Particle	Sanford-Wang parameter								
	c_1	c_2	c_3	c_4	c_5	c_6	c_7	c_8	c_9
π^+	206.4	1.030	5.902	2.012	2.127	5.510	0.9958E-01	12.03	
π^-	184.1	1.052	6.706	1.275	1.424	5.225	0.9439E-01	10.74	
K^+	12.53	1.654	0.314	1.038	0.174	4.658	0.106	10.53	2.635

Table 7: Central values for the Sanford-Wang $\pi^\pm$ and K^+ production used in the Dec04 baseline.

These sixteen parameters are chosen as in [8], and the cross-section tables are filled according to this Sanford-Wang parametrization.

`SWPar` : $\pi^\pm$ production is described according to two custom-defined Sanford-Wang parametrizations, where the user sets the value of the sixteen $\pi^\pm$ production parameters via the commands `/boone/physics/SWPiPlusPar` and `/boone/physics/SWPiMinusPar`. The cross-section tables for $\pi^\pm$ production are filled accordingly. K^+ production is described by a Sanford-Wang parametrization that is similar to the $\pi^\pm$ one, but with one extra parameter:

$$\frac{d^2\sigma(p+Be\rightarrow K^+ + X)}{dpd\Omega} = c_{k,1}p^{c_{k,2}}(1-\frac{p}{p_{beam}-c_{k,9}})\exp[-c_{k,3}\frac{p^{c_{k,4}}}{p_{beam}^{c_{k,5}}}-c_{k,6}\vartheta(p-c_{k,7}p_{beam}\cos^{c_{k,8}}\vartheta)] \tag{4}$$

where the nine parameters are set via the `/boone/physics/SWKaonPlusPar` command. The Sanford-Wang K^0_L production is based upon the K^+ one, times the GFLUKA K^0_L/K^+ production ratio in each (p_z, p_t) bin, similarly to what done Eq. 2.

The Dec04 baseline flux prediction assumes the `SWPar` model for $\pi^\pm$ and K^+ production, and the `MARS` model for secondary p, n, K^-, and K^0_L production. The default Sanford-Wang parameters are listed in Tab. 7. A lot of work in extracting these parameters has been done by Jocelyn Monroe, Jon Link, and Yan Liu. This work is summarized elsewhere, for example in Refs. [9], [10].

If the target material is not Beryllium, `BooNEG4Beam` also takes care of rescaling secondary particle production for all secondaries S, according to:

$$\frac{d^2N_{S,A}}{dp_z dp_t} \equiv (\frac{A(g/mol)}{9.01})^{c0+c1x_F+c2x_F^2} \tag{5}$$

where A is the atomic weight of the target material, $x_F = p_z/p_{beam}$, and $c0$, $c1$, $c2$ are parameters that can be set by the user via the command `/boone/physics/BeToAScalingPar`. The default values for these parameters are: $c0 = 0.74$, $c1 = -0.55$, $c2 = 0.26$. For Beryllium ($A = 9.01\ g/mol$), the rescaling function is one for all secondary p_z values.

We note that there are no requirements on conservation of quantities such as electric charge, baryon number, momentum, or energy, in inelastic interactions as described by `BooNEpBeInteraction`; the reason is threefold:

1. not all secondary particles are being produced, only the ones relevant to the neutrino fluxes;
2. as can be seen in Tab.6, different (and not necessarily consistent) models can be used for different secondaries;

Secondary particle type S	Average Multiplicity per inelastic collision	
	μ_S^{out}	μ_S^{in}
any	$(4.359 \pm 0.005) \cdot 10^0$	$4.362 \cdot 10^0$
p	$(1.544 \pm 0.002) \cdot 10^0$	$1.544 \cdot 10^0$
n	$(1.341 \pm 0.002) \cdot 10^0$	$1.343 \cdot 10^0$
π^+	$(7.99 \pm 0.01) \cdot 10^{-1}$	$7.99 \cdot 10^{-1}$
π^-	$(5.95 \pm 0.01) \cdot 10^{-1}$	$5.96 \cdot 10^{-1}$
K^+	$(4.79 \pm 0.02) \cdot 10^{-2}$	$4.79 \cdot 10^{-2}$
K_L	$(2.98 \pm 0.02) \cdot 10^{-2}$	$2.95 \cdot 10^{-2}$
K^-	$(2.65 \pm 0.06) \cdot 10^{-3}$	$2.65 \cdot 10^{-3}$

Table 8: Average multiplicity per inelastic collision for secondary particles produced in inelastic collisions of primary protons in a Be target. The μ_S^{out} column is obtained from the ntuple 102 output of a `BooNEG4Beam` simulation, the μ_S^{in} refers to the input to the simulation.

3. the algorithm in `BooNEpBeInteraction` described above for creating secondaries is meant to give reasonable results only in a statistical sense, not on an event-by-event basis. Of course, this should not have any effect on the MiniBooNE neutrino fluxes, which require the simulation of at least 10^6 protons on target. On the contrary, the absence of any requirements on particle correlations (in other words, the inclusive approach) makes it easier to interface additional experimental data to `BooNEG4Beam`, and is preferred.

A number of cross-checks have been made to make sure that the `BooNEpBeInteraction` class correctly describes particle production in p-Be inelastic interactions. We start by looking at the multiplicity per inelastic collision, μ_S, for the various secondary particle types $S = p, \pi^{\pm}, \ldots$.

In Tab.8, the average multiplicities for the Dec04 baseline parameters are given. The average multiplicities μ_S^{out} from the simulation of about $8 \cdot 10^5$ inelastic interactions is consistent with the simulation inputs μ_S^{in}, as it should be. As already mentioned, the average multiplicities μ_S per inelastic collision are obtained from the inclusive cross-section tables and the total inelastic cross-section σ_{inel}, via:

$$\mu_S = (\sum_{ipz=1}^{100} \sum_{ipt=1}^{50} \frac{\Delta^2 \sigma(p + Be \rightarrow S + X)}{\Delta p_z \Delta p_t})/\sigma_{inel} \tag{6}$$

for a secondary type S.

Having verified that the particle multiplicitites are as expected, we now examine the final state kinematics of the particles. Fig.3 shows the 2-dimensional (p_z, p_t) distributions for the momenta of the seven secondary particle types produced, p, $\pi^{\pm}$, $K^{\pm}$, K_L^0, and Fig. 4 the one-dimensional projections along the longitudinal and transverse momentum components. The histograms show the Dec04 baseline distributions, and the histogram statistics correspond to about $8 \cdot 10^5$ inelastic interactions [6].

[6] For protons and neutrons obtained from MARS, the p_t=1 GeV/c bin is meant to contain all overflow entries, but those protons and neutrons are actually generated with p_t =1 GeV/c in the simulation.

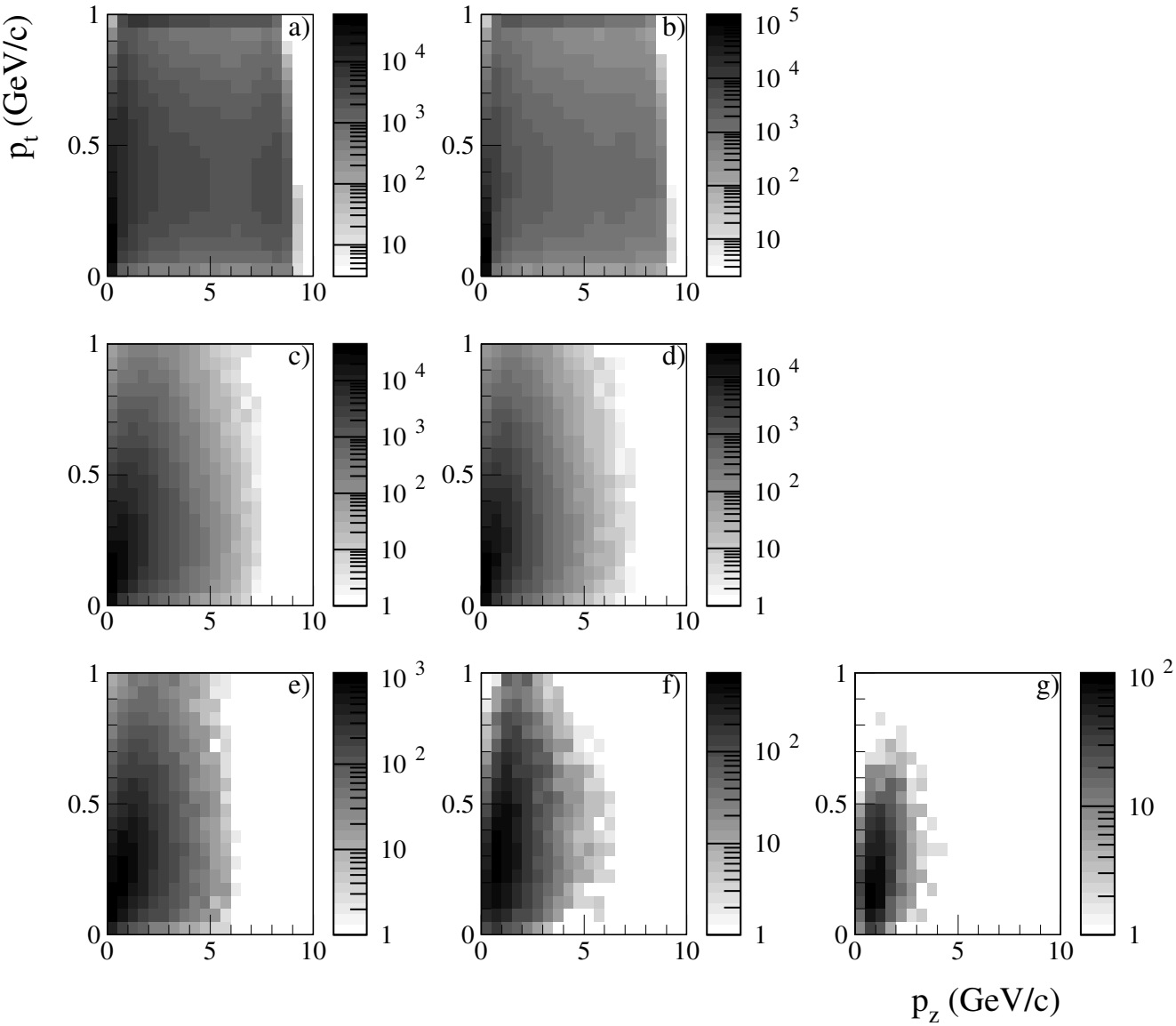

Figure 3: Two-dimensional histograms of the production momenta of secondary particles in inelastic collisions between primary protons and the MiniBooNE Be target, for the Dec04 baseline production. Histogram statistics refers to about $8 \cdot 10^5$ inelastic interactions. p_z is the longitudinal momentum with respect to the primary proton direction, p_t is the transverse momentum. The top row shows baryon production: panel a) is protons, b) is neutrons; the middle row shows non-strange neson production: panel c) is π^+, d) is π^-; the bottom row shows strange meson production: panel e) is K^+, f) is K^-, g) is K^0_L.

In the case of $\pi^\pm$ and K^+ production, we can directly compare the distributions in Fig.3 with the Sanford-Wang $\pi^\pm$, K^+ parametrizations discussed above. The ratios of the GEANT4 output distributions, divided by the distributions parametrized according to Eqs. 3, 4 and Tab.

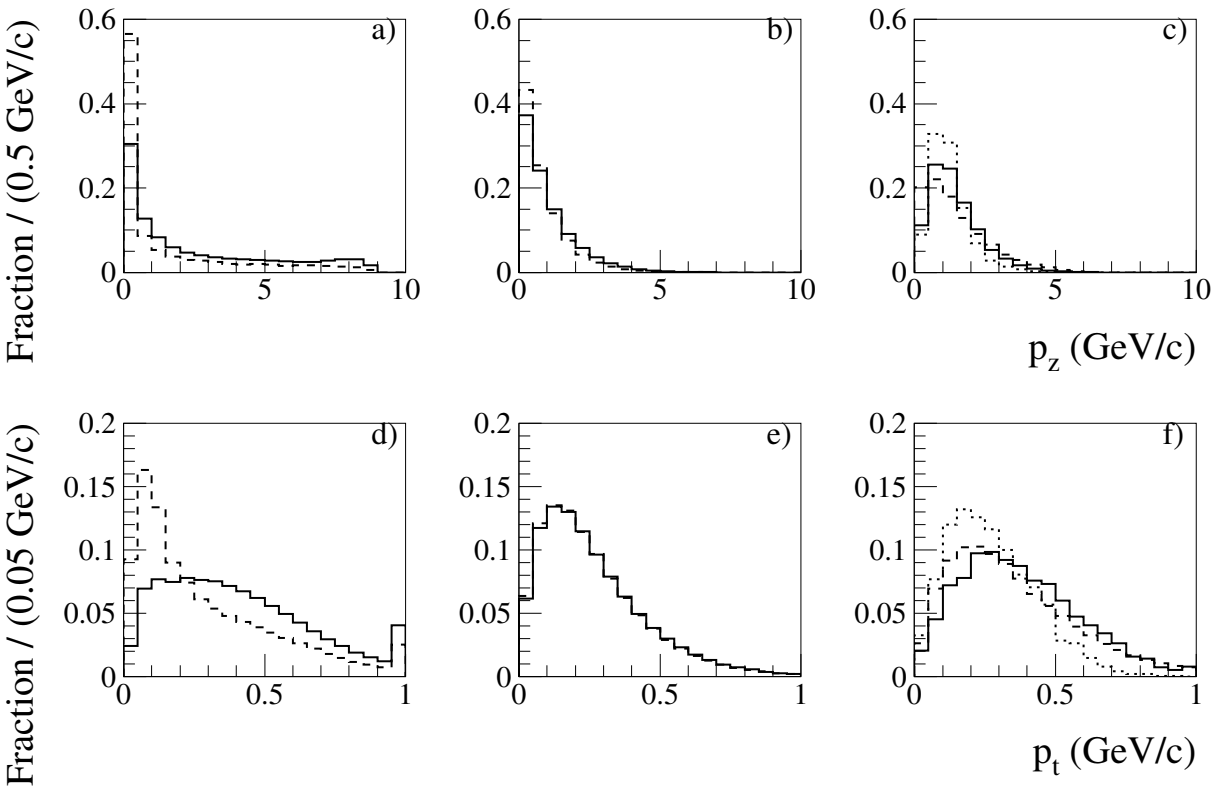

Figure 4: One-dimensional projections along the longitudinal and transverse momentum components p_z and p_t of the two-dimensional production histograms shown in Fig. 3. All histograms are normalized to unit area. The top (bottom) row shows the longitudinal (transverse) momentum distributions. Panels a) and d) refer to baryon production: solid histograms for protons, dashed histograms for neutrons; panels b) and e) refer to non-strange meson production: solid histograms for π^+, dashed histograms for π^-; panels c) and f) refer to strange meson production: solid histograms for K^+, dashed histograms for K^-, dotted histograms for K^0_L.

7, are shown in Fig.5. The distributions are normalized in order to represent the same number of inelastic interactions. We observe no systematic biases with respect to expectations in the `BooNEpBeInteraction` secondary momentum distributions.

6.3 Other inelastic processes

Secondary interactions of pions and protons play a non-negligible role in determining the MiniBooNE neutrino flux. These particles, once they have been created in a primary inelastic interaction, can still traverse significant amounts of target and horn material (relative to the inelastic interaction length, see Tab. 5), and in turn interact inelastically. Therefore, we study here inelastic interactions of secondary pions and protons of various momenta in Beryllium and Aluminum. These studies are made by defining pions and protons of various momenta as the G4 generated primaries, and studying their inelastic interactions in traversing simple geometries made of single

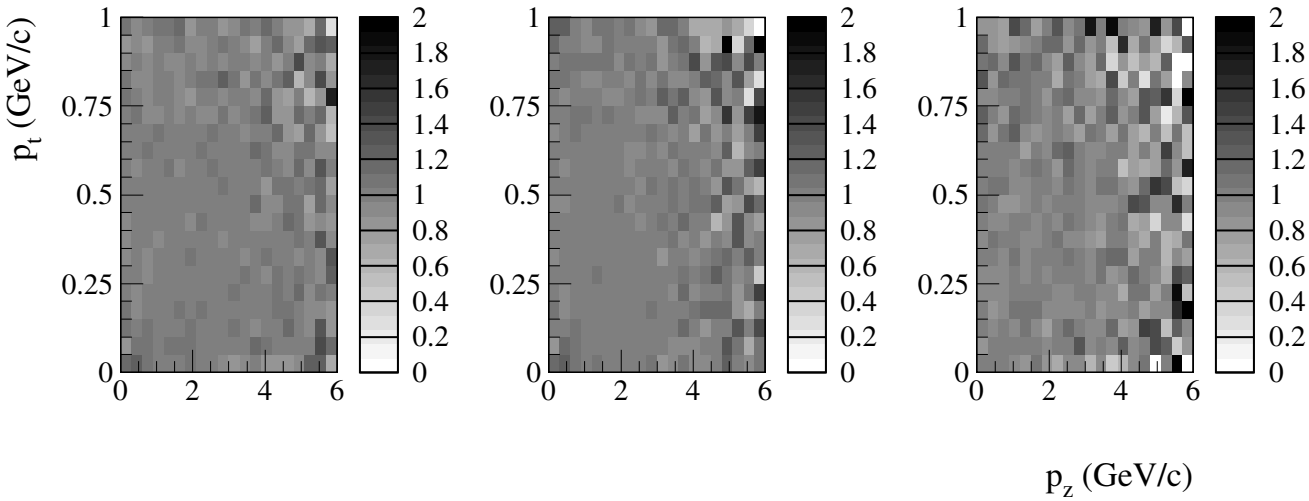

Figure 5: Cross-check on $\pi^{\pm}$ and K^{+} production multiplicity and kinematics, for inelastic collisions of primary protons in Be. Left plot: π^{+}; middle plot: π^{-}, right plot: K^{+}. The plots show the number of events in (p_z, p_t) bins of the produced pion/Kaon momentum, divided by the number of events in that bin given the number of inelastic collisions and final kinematics expected by the Sanford-Wang parametrizations of Eqs. 3 and 4, and Tab. 7. The 2D histograms are consistent with unity.

Beryllium or Aluminum volumes.

These inelastic processes, with the exception of $K_p > 7.5$ GeV protons in Beryllium discussed above, are described by the `G4LEPionPlusInelastic` and `G4LEProtonInelastic` classes (for the final state description), and by the `G4PiNuclearCrossSection` and `G4ProtonInelasticCrossSection` classes (for the total inelastic cross-section parametrization). The final state description classes are part of the 'Low Energy Parametrization Driven Model", based on the GEANT3.21 GHEISHA package (see the "Physics Reference Manual" at [4] for further details, or browse the source code at `$G4INSTALL/source/processes/hadronic/models/low_energy/`). The π^{+} charge exchange reaction is included in the inelastic reaction. The classes describing the total inelastic cross-section parametrizations are given in `$G4INSTALL/source/processes/hadronic/cross_sections/`.

Since release R1-10, it is possible to choose among alternative physics models describing the final state of hadronic interactions of proton, neutron, and pion secondaries. The alternative models currently implemented are the Bertini Intranuclear cascade model, and the binary cascade model (for details, see the "Physics Reference Manual" at [4]).

Figure 6 shows average properties of inelastic interactions of secondary π^{+}'s and protons in Beryllium and Aluminum, as a function of the projectile momentum. The average properties shown are:

1. inelastic interaction length, λ_{inel};
2. average number of π^{+}'s in the inelastic interaction final state, $\langle N_{\pi} \rangle$;

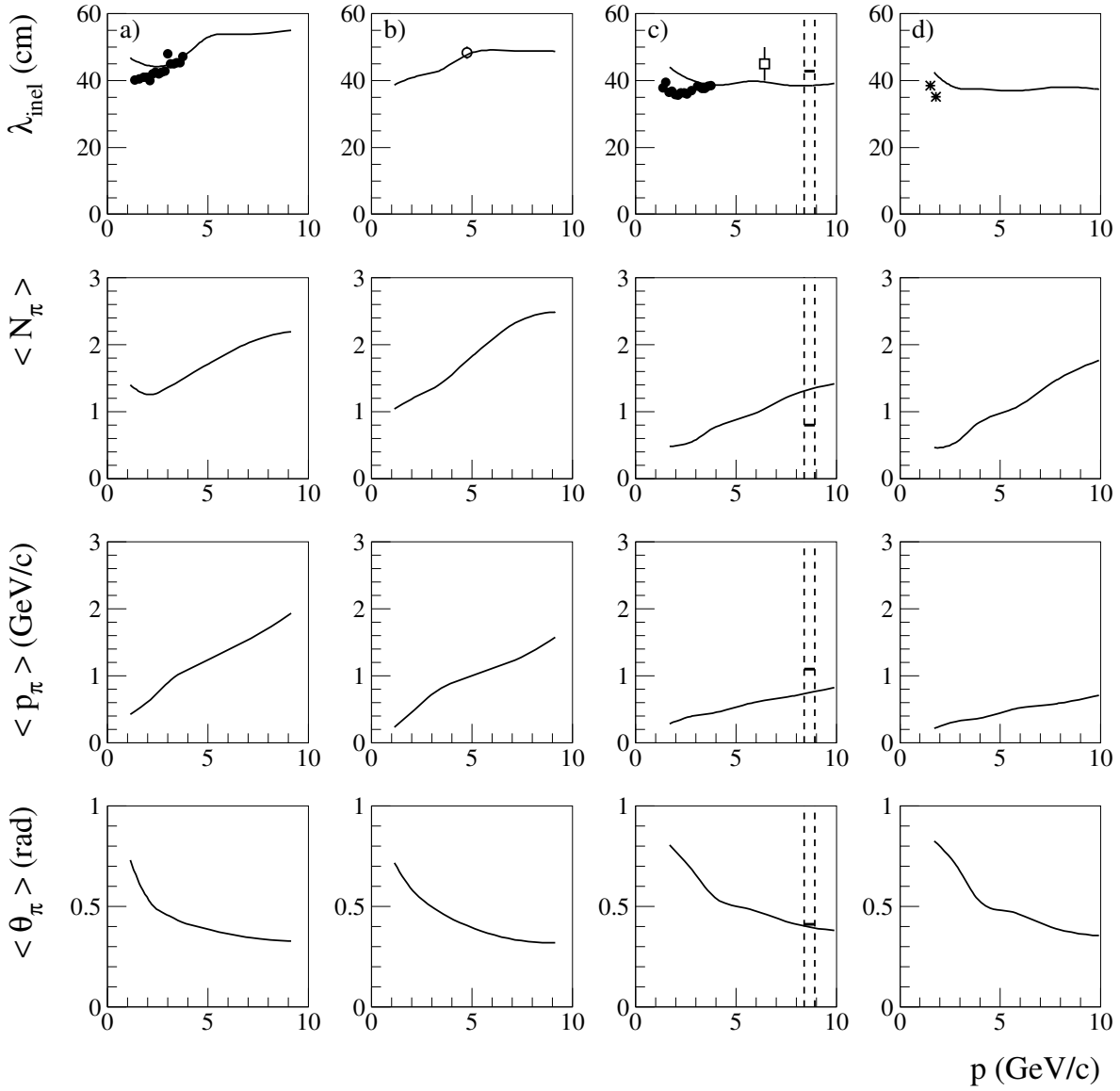

Figure 6: Cross-check on G4 inelastic processes for π^+'s and protons interacting in Beryllium and Aluminum, as a function of the projectile momentum p. From left to right: inelastic π^+-Be, π^+-Al, p-Be, and p-Al processes. From top to bottom: inelastic interaction length λ_{inel}, average number of final state π^+'s per inelastic collision $\langle N_\pi \rangle$, average momentum of final state π^+'s $\langle p_\pi \rangle$, average angle with respect to the projectile direction of final state π^+'s $\langle \vartheta_\pi \rangle$. Data: $\bullet$ from Ref. [13], $\circ$ from [14], $\square$ from [15], $*$ from [16]. The dashed vertical lines in the p-Be panels show the applicability range in proton momentum for the custom-defined inelastic cross-section of primary protons on Beryllium, and the horizontal segments within the dashed lines show the predictions from this model.

3. average momentum for final state π^+'s, $\langle p_\pi \rangle$;

4. average momentum direction for final state π^+'s, $\langle\theta_\pi\rangle$.

Experimental data are available on the total inelastic length, and are shown for comparison in Fig. 6. The `BooNEG4Beam` assumptions are within 10-15% of the measured values. The inelastic interaction lengths for π^+'s and protons are similar, of the order of 40-50 cm. The G4 inelastic cross-sections show a mild momentum dependence over the range $1 < p\ (GeV/c) < 10$.

Pions in the final state tend to be more numerous for higher energy projectiles, for π^+ projectiles than for p projectiles, and show little dependence on the target material. The average π^+ momenta tend to be much smaller than the projectile momenta, and π^+ emission angles are large. Note that the predictions for the inelastic model used for secondary proton interactions are not necessarily consistent with the predictions from the model used in primary proton inelastic interactions. The Dec04 Sanford-Wang parametrization for π^+ production predicts a smaller π^+ multiplicity, and a harder π^+ production spectrum, compared to the default GEANT4 low-energy model. As briefly mentioned above, the Dec04 baseline π^+ production assumption from 8.9 GeV/c protons on Beryllium is tied to a number of experimental data, not shown on this plot.

6.4 Elastic processes

Apart from scattering inelastically, pions and protons also interact elastically in the Be and Al materials. This process is simulated by the `G4LElastic` class. In this case, no particle absorption, particle production, or charge exchange occurs: the only effect is an angular deflection of the projectile with respect to its original direction. Therefore, we wish to study, as a function of projectile momentum:

1. what is the average distance travelled before an elastic interaction occurs in Beryllium and Aluminum? This is shown in the top plots of Fig.7;
2. what is the deflection angle with respect to the projectile direction when such elastic interactions occur? This is shown in the bottom plots of Fig.7;

The elastic interaction length is smaller in Aluminum than in Beryllium, and similar for protons or pions; moreover, the elastic interaction length tends to increase with projectile momemtum, in the $1 < p\ (GeV/c) < 10$ momentum range. Over this range, typical values in Beryllium are 110-205 cm, and 45-115 cm in Aluminum. significantly larger than the corresponding inelastic interaction lengths. Using the formula:

$$\frac{1}{\lambda_T} = \frac{1}{\lambda_{el}} + \frac{1}{\lambda_{inel}} \tag{7}$$

where λ_T is the total nuclear collision length, and the PDG values for λ_T and λ_{inel} at high-energy, $p > 60$ GeV/c [11], we get λ_{el} =117.0 and 77.7 cm for Be and Al, respectively. There is reasonable agreement between G4 and the PDG values for the p-Al elastic cross-section, less so for the p-Be one, with the G4 elastic interaction length 25% higher than the PDG value.

The mean deflection angles are much smaller in elastic collisions than in the previosuly discussed inelastic collisions (note that here the angles are expressed in mrad, not in rad!). The angles tend to be larger, on average, for low-energy projectiles, and are very similar for protons and pions. Typical deflection angles in one elastic collision are 10-150 mrad.

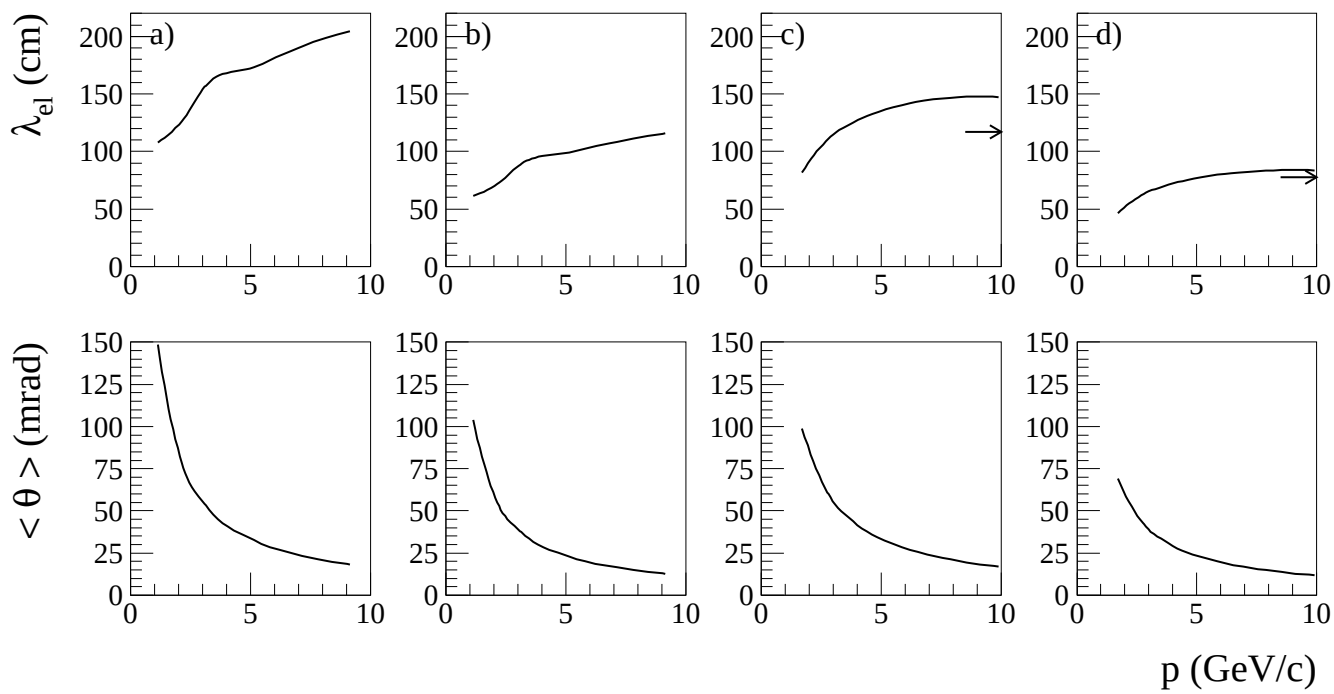

Figure 7: Cross-check on G4 elastic processes for π^+'sd and protons interacting in Beryllium and Aluminum, as a function of projectile momentum p. From left to right: elastic π^+-Be, π^+-Al, p-Be, and p-Al processes. Top plots: elastic interaction length λ_{el}; bottom plots: average projectile deflection angle $\langle\vartheta\rangle$. The arrows in the top plots indicate the high-energy values from [11].

6.5 Ionisation by charged hadrons

Having discussed the "microscopic" elastic and inelastic processes, we now turn to "macroscopic" effects of particle interactions in matter. We consider first energy loss processes by charged hadrons. The G4 class `G4hIonisation` simulates both the continuous energy loss due to ionisation and atomic excitation via the Bethe-Bloch formula, as well as the "discrete" part of the ionisation via δ-ray emission. We wish to study:

1. what is the energy loss of a pion or proton in traversing a certain material thickness?
2. what is the typical deflection angle due to ionisation after a certain material thickness?

We have simulated the ionisation characteristics for protons and π^+'s of various momenta in traversing 10 cm thick blocks of Beryllium and Aluminum. We define Δ as the projectile energy loss across the 10 cm of material:

$$\Delta \equiv -\int_0^{10\ \mathrm{cm}} \frac{dE}{dz} dz \tag{8}$$

Figure 8 shows the average values for Δ/z, where $z = 10$ cm, and for the deflection angle θ caused by energy loss processes.

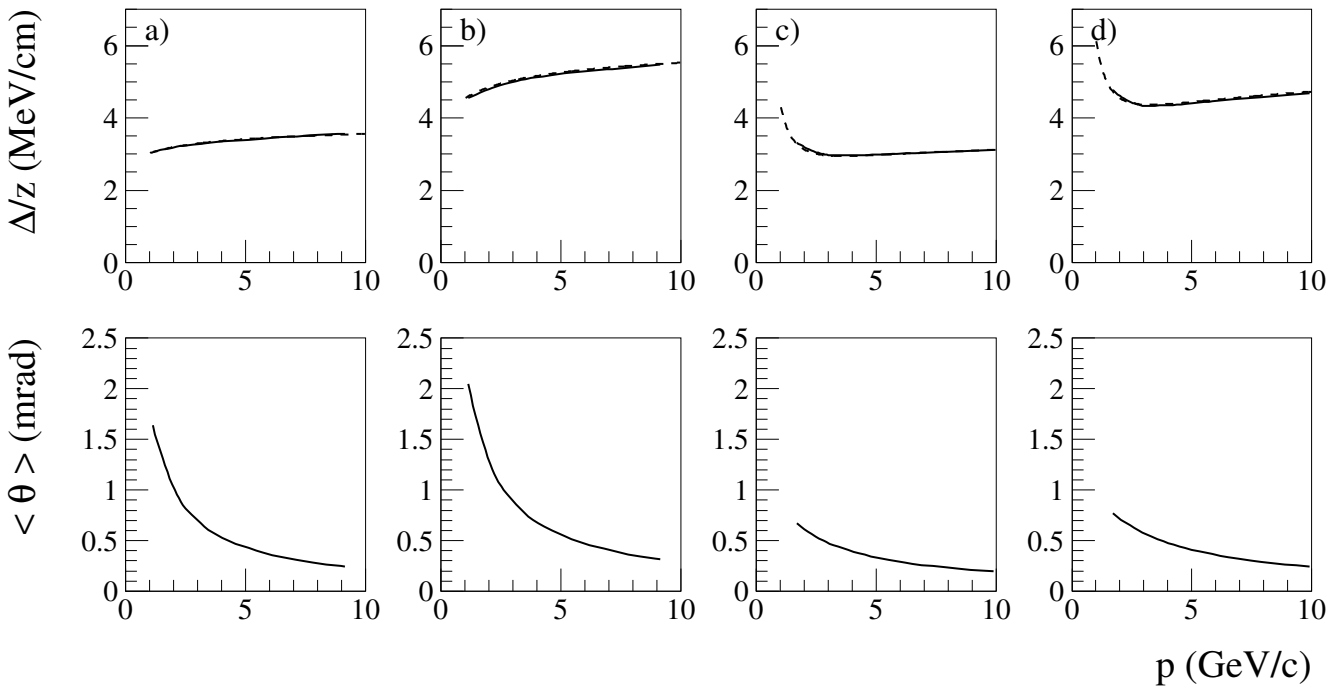

Figure 8: Energy loss results in GEANT4, obtained from a simulation of 10 cm of material, as a function of projectile momentum p. From left to right: energy loss of π^+ in Be, π^+ in Al, p in Be, p in Al. From top to bottom: average energy loss per unit material traversed, Δ/z; average projectile deflection angle, $\langle\theta\rangle$. The dashed curves, almost indistinguishable from the G4 solid curves, show the predictions from Eqs. 9 and 10 in the text.

The G4 energy loss results can be compared with the Bethe-Bloch formula given in [11], for π^+ or p projectiles in Be (Al):

$$-\frac{dE}{dx} = \rho K z^2 \frac{Z}{A}\frac{1}{\beta^2}[\frac{1}{2}\ln\frac{2m_e c^2\beta^2\gamma^2 T_{max}}{I^2} - \beta^2 - \frac{\delta}{2}] \tag{9}$$

where $K = 0.307075\ MeV\ g^{-1}\ mol^{-1}$, $z = 1$ is the projectile electric charge in units of e, $Z = 4$ (13) is the target electric charge in units of e, $A = 9.01$ (26.98) is the target atomic weight in units of g/mol, β is the projectile's velocity in units of c, $m_e c^2 = 0.511$ MeV is the electron mass, $\gamma = (1-\beta^2)^{-1/2}$, $T_{max} = 2m_e c^2\beta^2\gamma^2/(1 + 2\gamma m_e/M + (m_e/M)^2)$ is the maximum kinetic energy which can be imparted to a free electron in a single collision, $M = 139.57$ or $938.27\ MeV/c^2$ is the projectile's mass, $I = 63.7$ (166.0) eV is the mean excitation energy, and δ is the density effect correction to ionization energy loss, given by:

$$\delta = \begin{cases} 2(\ln 10)x - \bar{C} & \text{, if } x \geq x_1; \\ 2(\ln 10)x - \bar{C} + a(x_1 - x)^k & \text{, if } x_0 \leq x < x_1; \\ \delta_0 10^{2(x-x_0)} & \text{, if } x < x_0 \end{cases} \tag{10}$$

where $x = \log_{10}(p/Mc)$, x_0 =0.0592 (0.1708), x_1 =1.6922 (3.0127), $\bar{C}$ =2.7847 (4.2395), a =0.80392 (0.08024), k =2.4339 (3.6345), δ_0=0.14 (0.12). The expected energy loss given by Eqs. 9 and 10 is

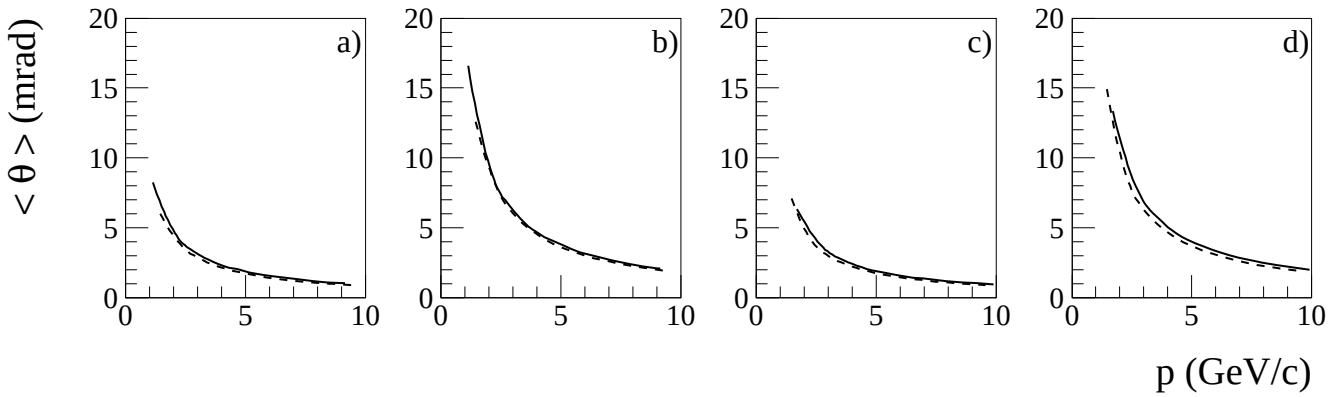

Figure 9: Multiple Coulomb scattering results in GEANT4, obtained from a simulation of 10 cm of material, as a function of projectile momentum p. From left to right: multiple Coulomb scattering of π^+ in Be, π^+ in Al, p in Be, p in Al. The average projectile deflection angle, $\langle\theta\rangle$, is shown. The dashed curves, almost indistinguishable from the G4 solid curves, show the predictions from Eqs. 11 and 12 in the text.

consistent with the G4 assumptions.

Figure 8 also shows the mean deflection angle after traversing 10 cm of material. These angles are very small, of the order of 1 mrad, and negligible with respect to the deflection angles due to nuclear elastic scattering or multiple Coulomb scattering, which we treat next.

6.6 Multiple Coulomb scattering

The cumulative effect of the many small electromagnetic scatters that a charged particle undergoes in matter is described by the `G4MultipleScattering` class. This model does not use the Molière formalism, but is based on the more complete Lewis theory [4]. As for the energy loss, we have simulated the effect of this process for pions and protons traversing 10 cm thick Be and Al blocks. We wish to know:

1. what is the scattering angle with respect to the original projectile direction, due to multiple Coulomb scattering (MCS)?

The scattering angle distributions for pions and protons of various momenta in Beryllium and Aluminum are shown in Fig.9.

Figure 9 gives the average G4 deflection angles due to multiple Coulomb scattering, $\langle\theta\rangle$, as a function of projectile momenta. GEANT4 predicts larger multiple Coulomb scattering angles for low-momentum projectiles, slightly larger scattering angles in Aluminum than in Beryllium, and larger scattering angles for protons with respect to pions of similar momentum. Typical scattering angles over 10 cm of material are between 1 and 20 mrad.

These results can be confronted with the Highland formula given by the PDG [11], describing the average MCS deflection angle $\langle\theta\rangle$:

$$\langle\theta\rangle_H = \sqrt{\frac{\pi}{2}}\sigma_\theta \tag{11}$$

where:

$$\sigma_\theta = \frac{13.6\ \text{MeV}}{\beta cp}\sqrt{z/X_0}[1 + 0.038\ln(z/X_0)] \tag{12}$$

In Eq.12, βc is the projectile velocity, p its momentum, $z \simeq 10$ cm is the material traversed, X_0 is the material radiation length, which is 35.28 cm for Be and 8.90 cm for Al [11]. In Fig. 9, the dashed curves show the average deflection angle due to multiple Coulomb scattering as predicted by the Highland formula: the G4 and Highland average deflection angles are consistent with each other.

6.7 Particle trajectories in horn magnetic field

The horn magnetic field provides a large ($\times 6$) increase in flux, and is therefore necessary to accurately check the motion of charged particles in the field. In GEANT4, as in GEANT3, the user has the capability to "attach" magnetic field attributes to a specific logical volume, in this case the horn logical volume "HRN1". In G4, this is done in the `BooNEGeometryConstruction` class. The magnetic field map is specified in the `BooNELocalField` class. The messenger class `BooNELocalFieldMessenger` allows the user to specify the horn current in the `jobOptions.in` file.

A quantitative cross-check of the G4 transportation algorithms through a non-uniform magnetic field region has been performed. The simple case considered is that of a magnetic field region that is similar to the MiniBooNE horn one, with an azimuthal fielld of magnitude $B = \mu_0 I/(2\pi r)$, where $\mu_0 = 4\pi \cdot 10^{-7}$ is the permittivity of free space, I =170 kA and $r = \sqrt{x^2 + y^2}$, in the region 2.2 cm $< r <$ 30 cm, $0 < z <$ 180 cm, and zero magnetic field otherwise. Positive pions of various momenta, produced at ($x = 0, y = 0, z = 30$ cm) and with an initial momentum direction of $p_x/p_z = 1/8,\ p_y = 0$, are tracked through this simple geometry both with a G4 simulation, and with an independent tracking program.

The independent tracking program assumes the following system of two coupled, second-order differential equations:

$$\begin{cases} \ddot{x}(t) = \frac{c_B}{x(t)}\dot{z}(t), & \dot{x}(0) = v_0 \sin\theta, \quad x(0) = x_0 \\ \ddot{z}(t) = -\frac{c_B}{x(t)}\dot{x}(t), & \dot{z}(0) = v_0 \cos\theta, \quad z(0) = z_0 \end{cases} \tag{13}$$

where, in SI units:

$$c_B = \frac{\mu_0 I}{2\pi} \cdot \frac{q}{m_\pi \gamma} \tag{14}$$

where μ_0 and I are defined as above, q is the (positive) electron charge, m_π the π^+ mass, γ is the relativistic γ factor for the pion, $v_0 = c\sqrt{\gamma^2 - 1}/\gamma$, $\theta = \arctan(1/8)$.

This set of equations does not seem analytically solvable, and a numerical integration method by Runge-Kutta-Nystrom is used instead, in order to check the G4 results. The implementation

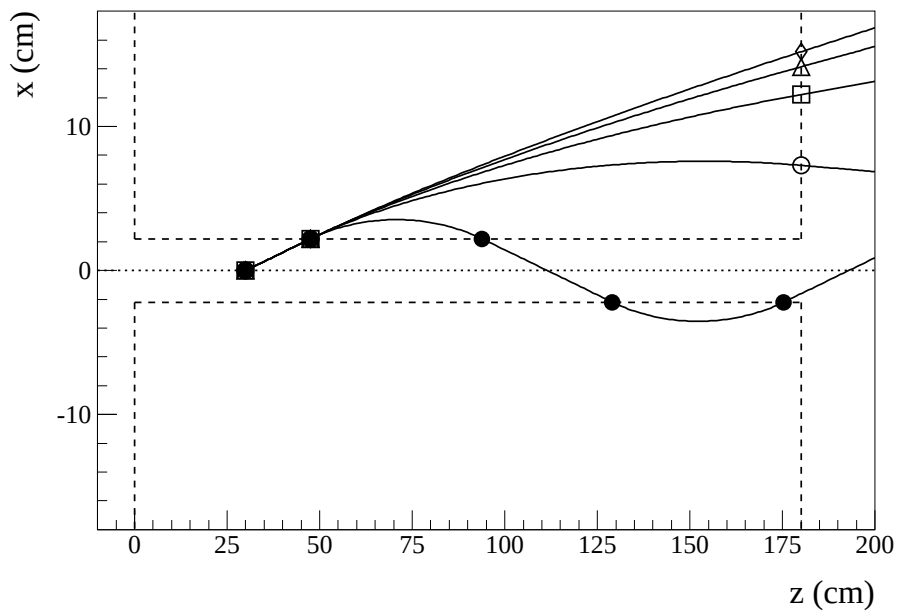

Figure 10: Trajectories in the horn magnetic field for 0.5, 1.5, 2.5, 3.5, and 4.5 GeV kinetic energy π^+'s, with initial conditions: ($x_0 = 0$, $z_0 = 30$ cm, $p_{x,0}/p_{z,0} = 1/8$). The dots are from a G4 simulation, the curves from the solution of Eq. 13 obtained with the CERNLIB subroutine `DRKNYS`.

used of this numerical method comes from the CERNLIB subroutine `DRKNYS`. The trajectories for as calculated by GEANT4 and by the CERNLIB program are shown in Fig.10, for 0.5, 1.5, 2.5, 3.5, 4.5 GeV kinetic energy positive pions. The G4 trajectories are consistent with the ones obtained by independently solving Eq. 13.

6.8 Particle decays

Neutrinos in the MiniBooNE detector are produced via the decays of charged pions, kaons, and muons. As far as particle decays are concerned, we wish to check:

1. what are the particles' lifetimes?
2. what are the decay branching ratios?
3. are Lorentz boosts implemented correctly?
4. what is the center-of-mass kinematics of the neutrinos produced in the decays?

In a typical beam Monte Carlo simulation, the output of `BooNEG4Beam` is fed into the redecay program `BooBeamNT`, originally written by Geoff Mills, and later modified by a number of people. The latter program redecays the neutrino parents a large number of times, with all decays occurring at the same parent decay vertex and according to the same decay channel as simulated by `BooNEG4Beam`. The program `BooBeamNT` is used for two reasons: first, large redecay factors (of the

Particle	Lifetime (ns)	Decay mode	Branching ratio (%)
π^+	26.03	$\mu^+\nu_\mu$	99.9877
		$e^+\nu_e$	0.0123
K^+	12.37	$\mu^+\nu_\mu$	63.17
		$\pi^+\pi^0$	21.2
		$\pi^+\pi^+\pi^-$	5.6
		$\pi^0 e^+\nu_e$	5.13
		$\pi^0\mu^+\nu_\mu$	3.2
		$\pi^+\pi^0\pi^0$	1.7
K^0_L	51.70	$\pi^0\pi^0\pi^0$	19.45
		$\pi^- e^+\nu_e$	20.4
		$\pi^+ e^-\bar{\nu}_e$	20.27
		$\pi^-\mu^+\nu_\mu$	13.55
		$\pi^+\mu^-\bar{\nu}_\mu$	13.46
		$\pi^0\pi^+\pi^-$	12.87
μ^+	2197.03	$e^+\nu_e\bar{\nu}_\mu$	100.0

Table 9: Particle lifetimes, and `BooNEG4Beam` decay modes and branching ratios.

order of 1000) are typically used to boost the neutrino flux statistics at the MiniBooNE detector with little additional cost in terms of CPU time requirements, since the propagation of neutrinos to the MiniBooNE detector is trivial: it is a very good approximation to assume no neutrino interactions, and simple straight line extrapolation from the neutrino production vertex to the detector. Second, it is known that GEANT4 does not simulate the neutrino kinematics in the three-body decays of Kaons and muons correctly. In particular, the correct $(V - A)$ theory is not applied to neutrinos (but only to charged leptons), and the muon polarization is not taken into account. This physics input is instead taken into account in the custom-defined routines of `BooBeamNT`. Therefore, the first two items in the list above (parent particle lifetimes and branching ratios) are set by `BooNEG4Beam`, while the latter two (Lorentz boosts and center-of-mass decay kinematics) are taken care of by `BooBeamNT`.

The user interface commands `/particle/property/dump` and `/particle/property/decay/dump` list the lifetimes and branching ratios used by the `BooNEG4Beam` code; those are reported in Tab.9 for π^+, K^+, K^0_L, and μ^+, together with the G4 classes responsible for simulating the decays. The built-in GEANT4 decay channels and branching ratios are used, apart from the following two exceptions:

- the decay $\pi^\pm \to e^\pm \overset{(-)}{\nu_e}$ has been added;
- the $K^\pm$ and K^0_L decay branching ratios have been modified according to latest values.

The `BooNEG4Beam` lifetime values are consistent with the PDG values [11], and the decay modes relevant for neutrino production are present at the expected branching ratios.

Next, we check the implenentation of Lorentz boosts. The relativistic time dilation of the neutrino parent lifetimes is simulated in `BooNEG4Beam`. Figure 11a) shows the decay length λ_{decay}

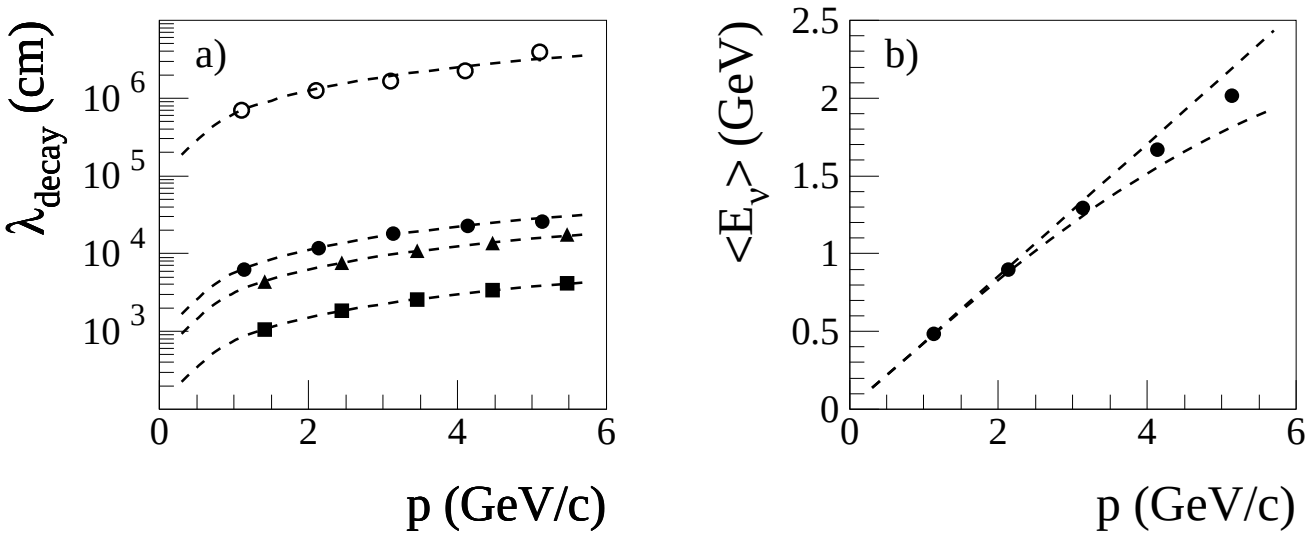

Figure 11: Validation of decay routines. Fig. 11a) shows the decay length λ_{decay}, obtained by fitting the distribution of the decay position to neutrinos, as a function of the parent momentum p, for π^+, K^+, K^0_L, μ^+ parents. Fig. 11b) shows the average neutrino energy in $\pi^+ \to \nu_\mu \mu^+$ decays as a function of pion momentum p, for neutrinos crossing the MiniBooNE detector. The points are the results from beam Monte Carlo simulations, the dashed curves are the predictions discussed in the text.

as a function of neutrino parent momentum p, for π^+, K^+, K^0_L, and μ^+ parents. The points are the average z-distributions from a `BooNEG4Beam` with only the transportation and decay processes activated. The dashed curves, consistent with the `BooNEG4Beam` results, show $\gamma\beta c\tau$, where the lifetime τ for a neutrino parent type is the one given in Tab. 9, and $\gamma\beta = p/m$, where m is the neutrino parent mass.

Lorentz transformations are applied by `BooBeamNT` to boost the neutrino 4-vector in the neutrino parent rest frame into the laboratory frame. In Figure 11b), we show the neutrino energy in the lab frame as a function of the parent neutrino momentum p in the lab frame, for $\pi^+ \to \mu^+\nu_\mu$ decays and for neutrinos crossing a disk of radius R_{det} =6.1 m and located L =541 m from the pion production location. The data points are obtained from a `BooBeamNT` simulation. The dashed curves correspond to maximum and minimum neutrino energy predictions, given by:

$$\begin{cases} E_{\nu,max} = \gamma E_\nu^{CM}(1+\beta) \\ E_{\nu,min} = \gamma E_\nu^{CM}(1+\beta\cos\theta^{CM}_{max}) \end{cases} \tag{15}$$

where: $E_\nu^{CM} = (m_\pi^2 - m_\mu^2)/(2m_\pi)$ is the neutrino energy in the pion rest frame, $\gamma = \sqrt{1+(p/m_\pi)^2}$, $\beta = \sqrt{\gamma^2-1}/\gamma$, $\theta^{CM}_{max} = 2\arctan(\gamma\tan\theta_{max})$ and $\theta_{max} = \arctan(R_{det}/L)$ are the angles between the pion direction and the neutrino directions in the pion rest frame and in the laboratory frame, respectively. From Fig. 11b), one finds that the average neutrino energy lies approximately in between the minimum and maximum energies from Eq. 15. This is because the neutrino decays isotropically in the pion rest frame ($dN/d\cos\theta^{CM} = const$), and therefore the neutrino energy

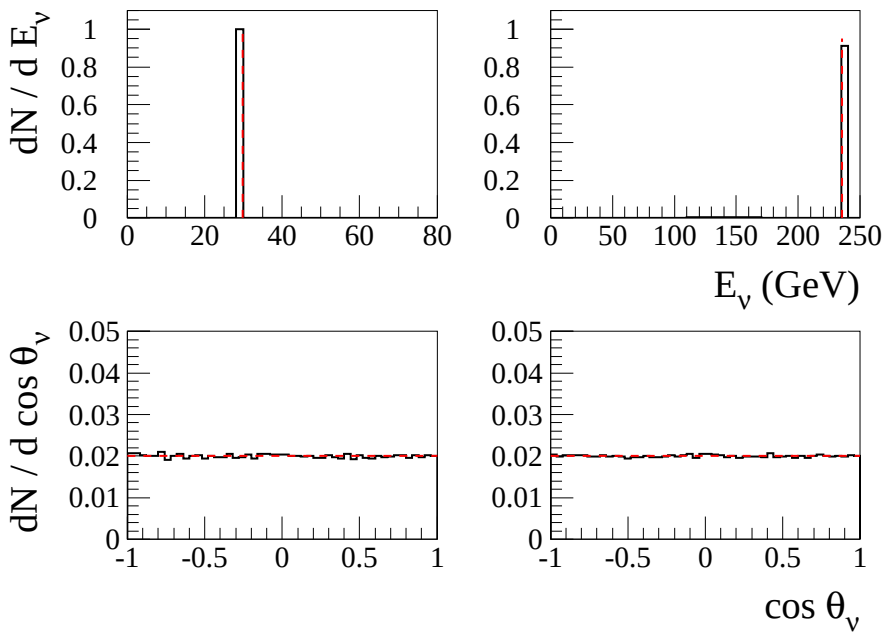

Figure 12: Muon neutrino kinematic distributions in the neutrino parent rest frame. The top row shows the neutrino energy distribution, the bottom row shows the neutrino angular distribution with respect to the z-direction in the lab frame. The left column refers to π^+ decays, the right column to K^+ decays. The histograms are the results of `BooBeamNT` simulations, the dashed curves are the predictions discussed in the text.

distribution in the laboratory is flat between $E_{\nu,min}$ and $E_{\nu,max}$ ($dN/dE_\nu = const$) [7].

Finally, we discuss the kinematics of neutrino decays in the rest frame of the neutrino parents, for the most relevant decays yielding muon and electron neutrinos. For the flux prediction, this part of the code is handled by `BooBeamNT`; therefore, we compare neutrino kinematic distributions from `BooBeamNT` simulations of neutrino parent decays at rest.

Muon neutrinos reaching MiniBooNE are mostly produced by π^+ decays, with a non-negligible contribution from K^+ decays (see Tab. 3). The histograms in Fig. 12 show the muon neutrino energy and angular distributions in π^+ and K^+ decays at rest. Both angular distributions are expected to be flat. The neutrino energy from the $\pi^+/K^+ \to \mu^+\nu_\mu$ two-body decays is $(m_{\pi/K} - m_\mu)/(2m_{\pi K})$. For Kaon decays, muon neutrinos with a continuous energy distribution can be obtained via the $K^+ \to \pi^0\mu^+\nu_\mu$ three-body decay, responsible for $BR(K^+ \to \pi^0\mu^+\nu_\mu)/(BR(K^+ \to \mu^+\nu_\mu) + BR(K^+ \to \pi^0\mu^+\nu_\mu)) \simeq 5\%$ of the muon neutrinos from K^+ decay (see Tab. 9). These expectations, shown with dashed curves in Fig. 12, agree well with the `BooBeamNT` results.

We now discuss muon decays and leptonic decays of Kaons (both charged and neutral), which are predicted to yield almost the entire electron neutrino flux at MiniBooNE (see Tab. 3). The

[7] Not quite: we have neglected the non-zero pion lifetime, and therefore the average L to consider should be slightly smaller.

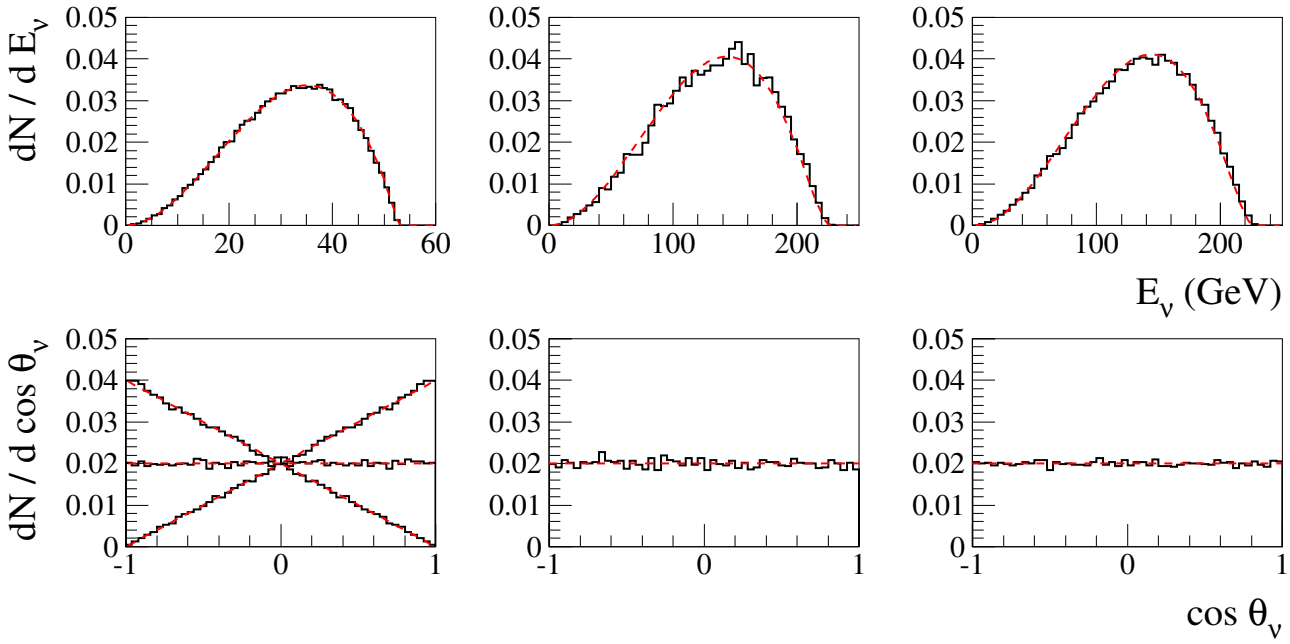

Figure 13: Electron neutrino kinematic distributions in the neutrino parent rest frame. The left column refers to μ^+ decays, the middle column to K^+ decays, and the right column to K_L^0 decays. The top row shows the neutrino energy distribution, the bottom row shows the neutrino angular distribution with respect to the z-direction in the lab frame, defined as the beam direction. The three curves for muons correspond to the cases: $P_z = -1, 0, +1$, where P_z is the projection along z of the muon polarization vector in the muon rest frame. he histograms are the results of `BooBeamNT` simulations, the dashed curves are the predictions discussed in the text.

neutrino energy and angular distribution from μ^+ decays is, neglecting terms proportional to the electron mass [17]:

$$\frac{dN}{dx d\cos\theta_\nu} \propto \frac{12x^2}{4\pi}(1-x)(1 \mp P_z \cos\theta) \tag{16}$$

where $\cos\theta_\nu$ is the neutrino emission angle with respect to the beam direction z, P_z is the projection along z of the muon polarization vector in the muon rest frame, and $x = 2E_\nu/m_\mu$, with $0 < x < 1$. In $\pi^+ \to \mu^+\nu_e$ decays, the muon polarization in the muon rest frame is calculated by `BooNEG4Beam` from the known muon polarization in the pion rest frame, boosting the polarizaton vector into the muon rest frame.

For the Kaon three-body decays yielding electron neutrinos (that is, $K \to \pi e \nu_e$, or K_{e3} decays), the neutrino angular distribution, in the Kaon rest frame and with respect to the beam direction, is expected to be flat. Assuming that only the vector current contributes to the Kaon semileptonic decay matrix element, and neglecting electron mass terms, the neutrino energy distribution in the Kaon rest frame is [18]:

$$\frac{dN}{dE_\nu} \propto \int_{E_{e,-}}^{E_{e,+}} dE_e (2E_e E_\nu - m_k E'_\pi)|f_+(t)|^2 \tag{17}$$

where all quantities refer to the Kaon rest frame, E_e is the electron energy, $E'_\pi \equiv E_\pi^{max} - E_\pi$, $E_\pi^{max} = (m_K^2 + m_\pi^2)/(2m_K)$ is the maximum energy that can be transferred to the pion, E_π is the pion energy, f_+ is a form factor depending only on the square of the four-momentum transfer to the leptons, $t = (p_k - p_\pi)^2 = m_k^2 + m_\pi^2 - 2m_k E_\pi$, and $E_{e,\pm}$ are integration limits on the electron energy:

$$\begin{cases} E_{e,-} = \frac{m_K^2 - m_\pi^2}{2m_k} - E_\nu \\ E_{e,+} = \frac{1}{2}(m_k - \frac{m_\pi^2}{m_k - 2E_\nu}) \end{cases} \tag{18}$$

and we also assume, as customarily done, a linear dependence of the form factor f_+ on t:

$$f_+(t) \propto (1 + \lambda_+ t/m_\pi^2) \tag{19}$$

For K_{e3}^+ (K_{e3}^0) decays, the coefficient λ_+ for the linear expansion of the form factor is taken to be 0.0277 (0.0291) from Ref. [11].

The expected kinematics for electron neutrinos in muon decays and semileptonic Kaon decays described above are shown with dashed lines in Fig. 13, and agree well with the `BooBeamNT` results.

7 Pion fluxes

In the previous Section we have discussed the validation of the physics processes of greatest relevance to MiniBooNE, as implemented in `BooNEG4Beam` and `BoobeamNT`, one by one; in this way, the simulation outcomes could often be confronted with simple analytical predictions. Now we wish to cross-check the combined effect of most of these physics processes, together with the MiniBooNE geometry and primary proton description discussed in Section 4. In order to do this, we compare the beam Monte Carlo results with the ones obtained from an independent simulation program, `Model_B`.

7.1 `Model_B`: a brief description

`Model_B` is a MiniBooNE beam simulation program written by Mike Shaevitz. `Model_B` takes into account the most important effects shaping the MiniBooNE ν_μ flux. The program loops over the pion production location, pion momentum and angle at prooduction from p-Be interactions in the target, and maps this pion spectrum into a neutrino energy spectrum at the MiniBooNE detector. This is done by using numerical integration techniques that are more "transparent" to the user than the techniques used in a complicated Monte Carlo program such as GEANT4. The physics taken into account in the following `Model_B` comparisons is:

1. interaction length for p-Be inelastic interactions, identical to the `BooNEG4Beam` one;
2. π^+ production in p-Be inelastic interactions, according to a Sanford-Wang parametrization identical to the `BooNEG4Beam` one given in Tab. 7;
3. π^+ absorption in the Beryllium and Aluminum material traversed by the pion. The absorption length is modelled as the average of the inelastic and elastic interaction lengths as a function of material and pion momentum, obtained from `BooNEG4Beam`. The rationale for using this average is to include the effect of all inelastic reactions as well as that of elastic scattering at large angles, into absorption, since `Model_B` does not simulate the final state from pion interactions;
4. π^+ raytracing in the horn magnetic field. The trajectory is calculated numerically using the Runge-Kutta method in the CERNLIB routine `DRKNYS`, as described in the previous Section;
5. path length that a focused pion trajectory would traverse in air before hitting the collimator, decay pipe walls, or beam absorber materials, if no pion decays were present;
6. $\pi^+ \to \mu^+\nu_\mu$ decay;
7. the phase space acceptance for the pion to decay into a ν_μ that hits the MiniBooNE detector.

In this section, we compare the pion fluxes at different locations along the MiniBooNE beamline from `Model_B` and this simplified version of `BooNEG4Beam`; the neutrino flux comparison is discussed in the next Section. The `Model_B` code used to make these comparisons is the one available in CVS (in the `ModelBeam` directory), with minor modifications to match the Dec04 baseline values used in `BooNEG4Beam` for the total p-Be inelastic cross-section and for the Sanford-Wang π^+ production parametrization.

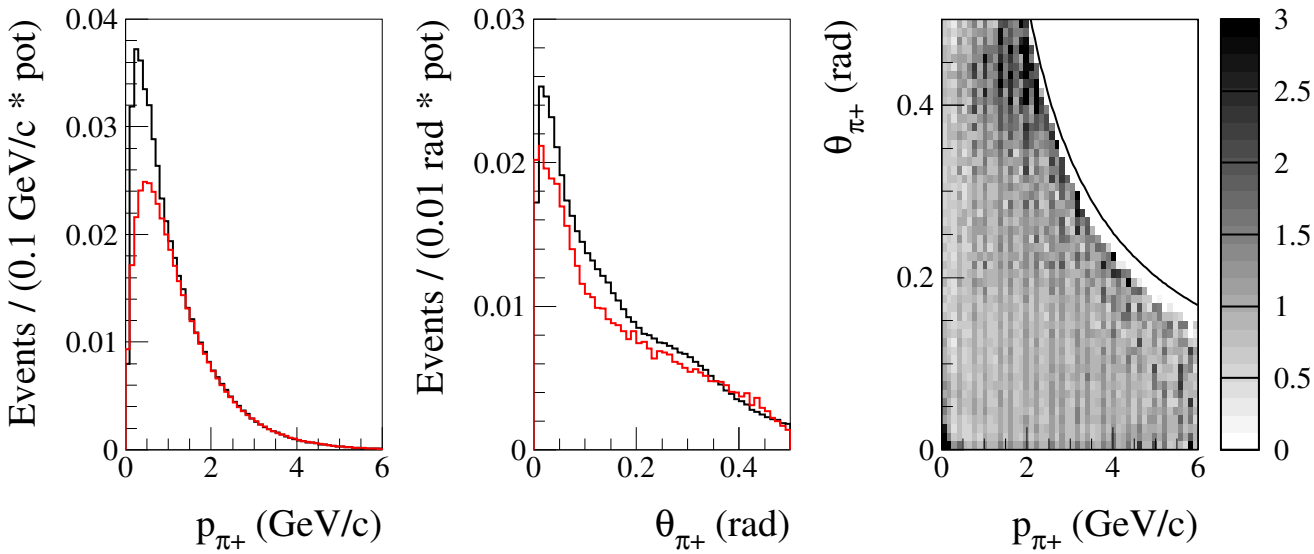

Figure 14: `Model_B`/`BooNEG4Beam` comparisons of pion fluxes after the horn. The pion momentum p_{π^+} and angle θ_{π^+} distributions are shown in black for `BooNEG4Beam`, in red for `Model_B`. The right scatter plot in the $(p_{\pi^+}, \theta_{\pi^+})$ plane shows the ratio between the `Model_B` and `BooNEG4Beam` yields. The solid curve is for $p_t = 1$ GeV/c, the maximum p_t value sampled in `BooNEG4Beam`.

Position	$N_{\pi+}$/pot		$\langle p_{\pi+,in} \rangle$ (GeV/c)		$\langle \vartheta_{\pi+,in} \rangle$ (mrad)	
	Model_B	G4	Model_B	G4	Model_B	G4
After horn	0.412	0.485	1.23	1.11	165	158
After collimator	0.121	0.164	1.47	1.28	36	60

Table 10: Summary on `Model_B`/`BooNEG4Beam` comparisons of pion fluxes, after the horn and after the collimator. The pion fluxes per proton on target, the average pion momentum and angle are given at both planes, for both `Model_B` and `BooNEG4Beam`.

7.2 Pion fluxes after the horn

A `Model_B`/`BooNEG4Beam` comparison of pion fluxes after the horn, at $z = 200$ cm where $z = 0$ indicates the upstream face of the horn, is useful to check (mostly) pion production and pion focusing in the horn magnetic field. Number of pions, and the distributions of pion momenta and angles are shown in Fig.14; the mean values for these quantities are given in the "After horn" row in Tab.10

The agreement is good above $p_\pi > 1.5$ GeV/c, while `BooNEG4Beam` predicts significantly more low-energy pions after the horn. A hypothesis (to be checked) is that those low-energy pions are due to $p \to p \to \pi^+$ processes (the arrow indicates an inelastic interaction), not simulated by `Model_B`. Also, the different treatment of pion reinteractions in the two programs might play a significant role.

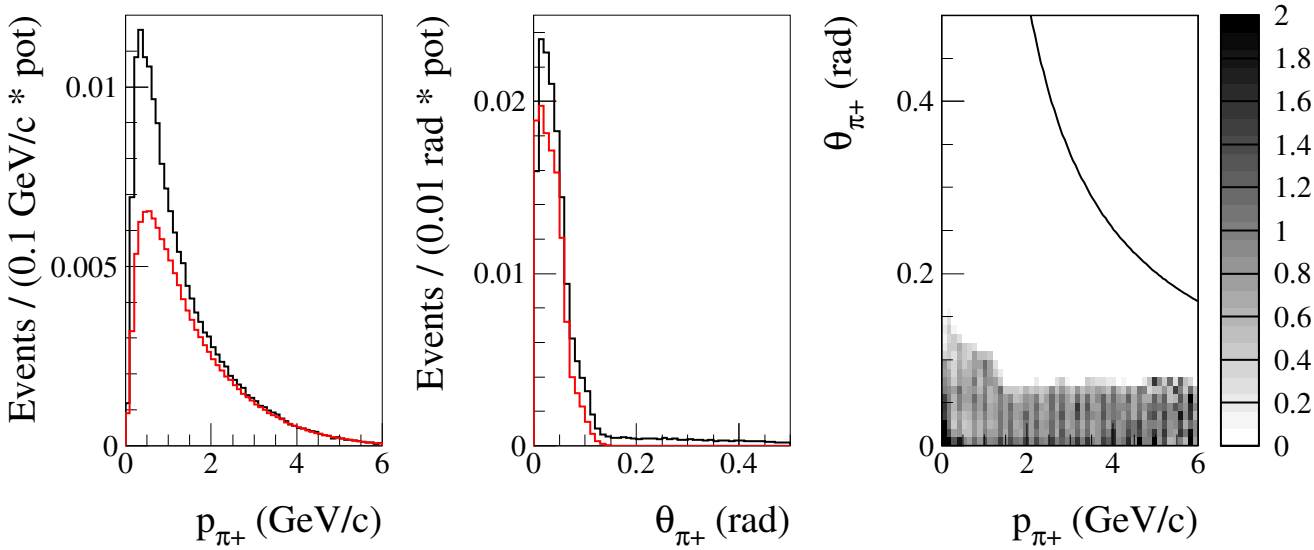

Figure 15: `Model_B`/`BooNEG4Beam` comparisons of pion fluxes after the collimator. The pion momentum p_{π^+} and angle θ_{π^+} distributions are shown in black for `BooNEG4Beam`, in red for `Model_B`. The right scatter plot in the $(p_{\pi^+}, \theta_{\pi^+})$ plane shows the ratio between the `Model_B` and `BooNEG4Beam` yields. The solid curve is for $p_t = 1$ GeV/c, the maximum p_t value sampled in `BooNEG4Beam`.

7.3 Pion fluxes after the collimator

The collimator system provides additional pion focusing along the beam direction. Pion yields and momentum distributions from `BooNEG4Beam` and `Model_B` in a plane downstream of the cone collimator are compared in Fig.15. The plane is defined as the $z = 560$ cm plane in global coordinates. The motivation for type of check is similar to the one after the horn, but places more emphasis on the pions that ultimately matter to MiniBooNE.

The comparison of the distributions in Fig.15 is summarized in the "After collimator" row in Tab.10. The same trend seen after the horn is visibile here, as well, with `BooNEG4Beam` predicting significantly more low-energy pions, and good agreement for high-energy pions. Also, the `BooNEG4Beam` angular distribution of pions after the collimator is significantly broader than the `Model_B` one.

The comparisons shown in this Section, while more difficult to interpret than the ones given in Section 6, show that the `BooNEG4Beam` predictions can be reproduced reasonably well by an independent, analytic program such as `Model_B`, indicating that most of the relevant physics affecting the pion fluxes can be identified and their effect quantified. Nevertheless, significant differences between the `BooNEG4Beam` and `Model_B` simulation results are present, and should be understood, both to validate the `BooNEG4Beam` code, and for perfecting the `Model_B` predictions.

8 Neutrino fluxes at the MiniBooNE detector

The final results of a MiniBooNE Monte Carlo, and the only ones that ultimately matter, are the predictions for the neutrino fluxes at the MiniBooNE detector. In this Section we discuss:

1. comparisons on the ν_μ flux between `Model_B` and `BooNEG4Beam`;
2. results on the fluxes of all neutrino flavors for the Dec04 baseline;

Large pion decay statistics is needed in order to produce smooth distributions as a function of neutrino energy in the small solid angle subtended by the MiniBooNE detector; for this reason, the results from the `BooNEG4Beam` simulations shown in this Section are obtained by redecaying all neutrino-producing parent particles 1000 times via the `BooBeamNT` decay simulator program discussed in the decay part of Section 6. All fluxes are obtained considering neutrinos crossing a 6.1 m radius circle centered on the beam axis and located 541 m downstream of the target.

8.1 Comparison of `BooNEG4Beam`/`Model_B` neutrino fluxes at the detector

Fig.16 shows the ν_μ fluxes predicted by `Model_B` and `BooNEG4Beam` (see Section 7 for details on `Model_B`).

Simulation	ϕ_{ν_μ} $(10^{-10}/(cm^2 \cdot \text{pot}))$	$\langle E_\nu \rangle$ (GeV)	$\langle p_{\pi+,in} \rangle$ (GeV/c)	$\langle \vartheta_{\pi+,in} \rangle$ (mrad)	$\langle p_{\pi+,out} \rangle$ (GeV/c)	$\langle \vartheta_{\pi+,out} \rangle$ (mrad
`Model_B`	4.71	0.826	2.21	98	2.21	20
`BooNEG4Beam` ($p \to \pi^+ \to \nu_\mu$ only)	4.16	0.769	2.17	106	2.08	30
`BooNEG4Beam` (all ν_μ processes)	4.83	0.776				

Table 11: Summary on `Model_B`/`BooNEG4beam` comparisons of the ν_μ flux at the MiniBooNE detector. The overall ν_μ flux ϕ_{ν_μ}, as well as the average neutrino energy ($\langle E_{\nu_\mu} \rangle$), pion production momentum ($\langle p_{\pi^+,in} \rangle$), production angle ($\langle \theta_{\pi^+,in} \rangle$), pion momentum at decay ($\langle p_{\pi^+,out} \rangle$) and angle at decay ($\langle \theta_{\pi^+,out} \rangle$), for pions giving neutrinos in MiniBooNE are given for both `Model_B` and `BooNEG4Beam`. The average values are to be intended as averages over the ν_μ flux distribution.

While the two programs predict similar overall muon neutrino fluxes, $4.71 \cdot 10^{-10}$ and $4.83 \cdot 10^{-10}$ $(cm^2 \cdot pot)^{-1}$ respectively, at a closer look there are noticeable differences. First, only muon neutrinos from $p \to \pi^+ \nu_\mu$ in `BooNEG4Beam` should be compared to the `Model_B` predictions, since `Model_B` only simulates this process. For this comparison, the `BooNEG4Beam` flux prediction is about 12% lower than the `Model_B` one. Second, again restricting the comparison to $p \to \pi^+ \nu_\mu$ events only, the `BooNEG4Beam` neutrino energy averaged over the flux distribution is 50-60 MeV (or 7%) lower than the `Model_B` one. This effect is not due (at least for the most part) to ionization processes that are simulated in `BooNEG4Beam` and not in `Model_B`; this is shown by the blue histogram in Fig. 16, giving the `BooNEG4Beam` $p \to \pi^+ \to \nu_\mu$ flux prediction without π^+ ionization. It is unlikely that the discepeancy is due to multiple Coulomb scattering either, since typical MCS deflections angles are of the order of a few mrad, for $\simeq 2$ GeV/c pions traversing few cm of Beryllium and Aluminum (see Section 6). To conclude, the discrepancies between the two programs are of the order of 10%,

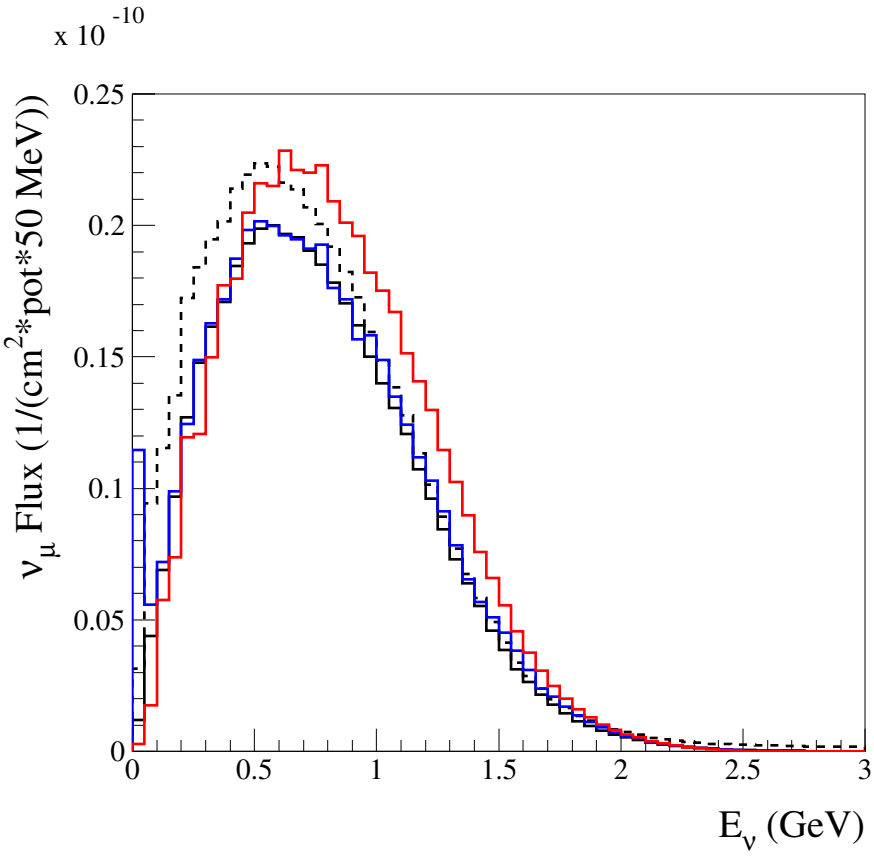

Figure 16: ν_μ flux as a function of neutrino energy E_ν predicted by the same π^+ production model in BooNEG4Beam (solid black, dashed black, and solid blue) and in Model_B (red). The dashed black BooNEG4Beam histogram corresponds to the entire muon neutrino flux prediction, the solid black and solid blue histograms to the muon neutrino flux from $p \to \pi^+\nu_\mu$ only, with and without hadronic ionization processes activated for positive pions, respectively.

and those are not understood.

In Fig.17 and Tab.11 we also show the pion momentum and angle distributions at pion production, and Tab. 11 also gives the average pion momenta and angles at decay, for pions producing neutrinos in the MiniBooNE detector via $p \to \pi^+\nu_\mu$ processes only. The level of agreement is similar to the one seen for neutrino energy distributions. Model_B predicts slightly greater average values for the pion momenta, and smaller angles. This discrepancy in pion angles is likely to be responsible for the slighlty harder Model_B neutrino energy distribution.

In Fig.,17, we also show the curve corresponding to $p_t = 1$ GeV/c in the $(p_{\pi^+}, \theta_{\pi^+})$ plane. As explained in Section 6, in BooNEG4Beam the pion production is parametrized in terms of longitudinal and transverse momentum: Fig.17 shows that the upper limit of 1 GeV/c used for the p_t sampling is sufficient, as only a negligibly small fraction of pions of higher transverse momenta produce neutrinos in the MiniBooNE detector. This conclusion holds true for other mesons as

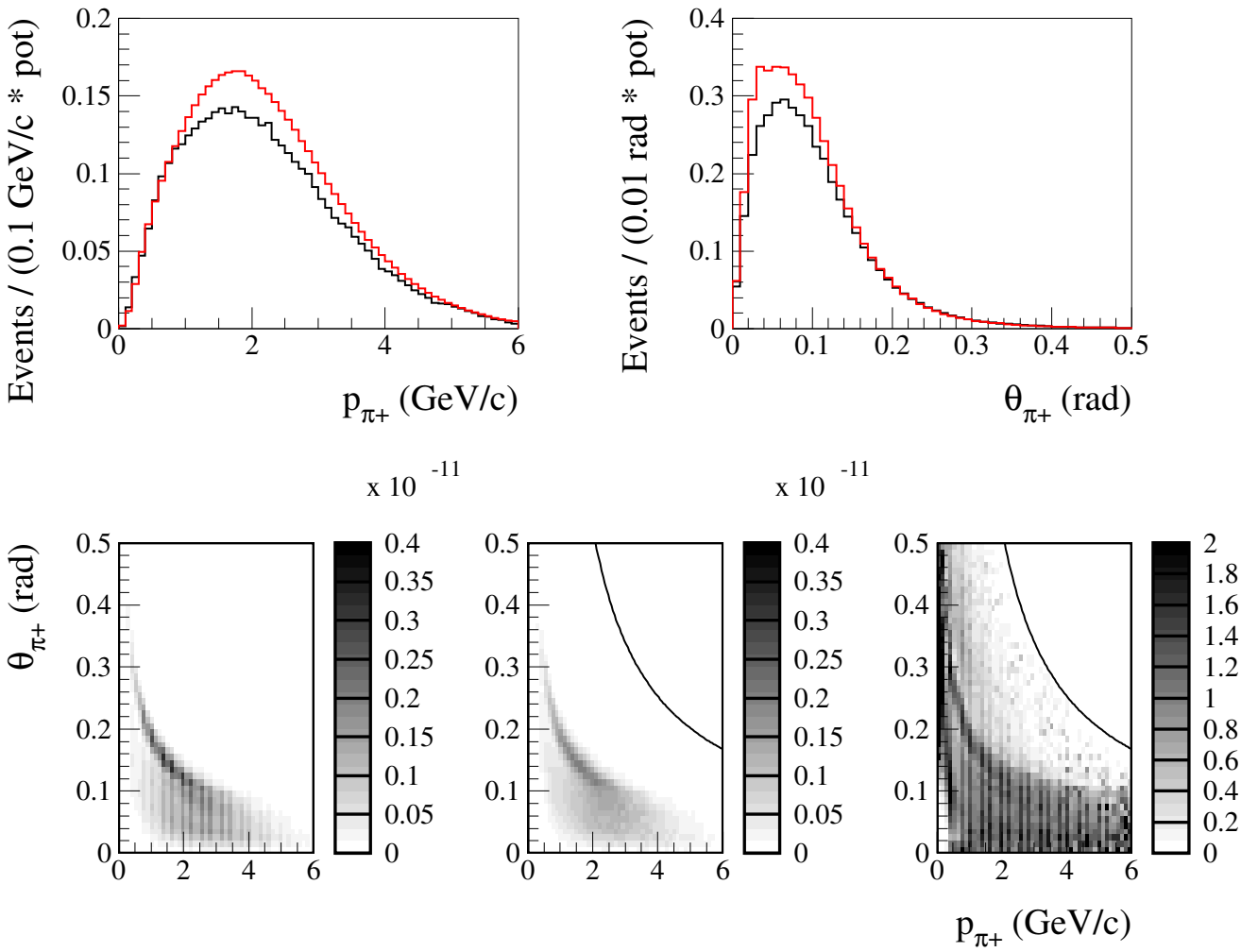

Figure 17: Model_B/BooNEG4Beam comparisons on the pion momentum (p_{π^+}) and angle (θ_{π^+}) at production, for pions giving neutrinos in the MiniBooNE detector via $p \to \pi^+\nu_\mu$. The top two plots show the BooNEG4Beam histograms in black, the Model_B histograms in red. The bottom left and middle plots show the same $p_{\pi^+}, \theta_{\pi^+}$ quantities in a scatter plot, for Model_B and BooNEG4Beam, respectively. The bottom right plot shows the ratio of the Model_B yields divided by the BooNEG4Beam yields in the $(p_{\pi^+}, \theta_{\pi^+})$ plane. The black curve in the bottom middle and right plots shows the $p_t = 1$ GeV/c curve.

well. Moreover, the shape of the 2-dim histograms in Fig. 17 motivates why BooNEG4Beam samples secondary particle production momenta in terms of (p_z, p_t), and not (for example) (p, θ): most of the pions relevant to MiniBooNE are produced in a relatively narrow p_t range, but wider θ range.

8.2 Dec04 neutrino flux predictions from BooNEG4Beam/BooBeamNT

We conclude this Section by giving the Dec04 baseline flux predictions obtained with the BooNEG4Beam and BooBeamNT programs, for neutrino running mode.

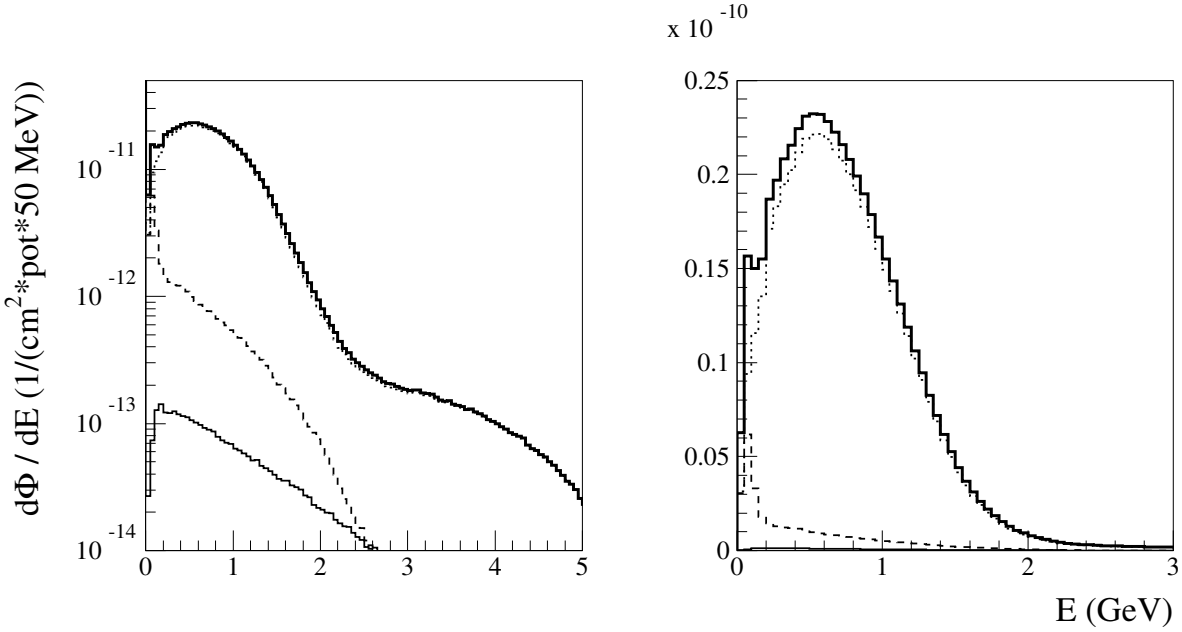

Figure 18: Predicted neutrino flux as a function of neutrino energy, for all neutrinos reaching MiniBooNE, in neutrino running mode. The thick solid histogram is for all neutrinos, the thin solid histogram for ν_e, the dashed histogram for $\bar{\nu}_\mu$, the dotted histogram for ν_μ. The fluxes are shown on a logarithmic scale on the left, and on a linear scale on the right.

Neutrino Flavor	Neutrino Parent	ϕ ($cm^{-2}pot^{-1}$)	$\langle E_\nu \rangle$
all	all	$5.22 \cdot 10^{-10}$	0.760
ν_μ	all	$4.84 \cdot 10^{-10}$	0.778
ν_μ	π^+	$4.69 \cdot 10^{-10}$	0.734
ν_μ	K^+	$1.42 \cdot 10^{-11}$	2.250
$\bar{\nu}_\mu$	all	$3.47 \cdot 10^{-11}$	0.488
$\bar{\nu}_\mu$	π^-	$3.24 \cdot 10^{-11}$	0.470
ν_e	all	$3.07 \cdot 10^{-12}$	0.939
ν_e	μ^+	$1.70 \cdot 10^{-12}$	0.665
ν_e	μ^+	$1.07 \cdot 10^{-12}$	1.321
$\bar{\nu}_e$	all	$3.44 \cdot 10^{-13}$	0.888
$\bar{\nu}_e$	K^0_L	$2.55 \cdot 10^{-13}$	1.032

Table 12: Summary of neutrino flux predictions at MiniBooNE, for neutrino running mode. The fluxes ϕ, as well as the neutrino energy $\langle E_\nu \rangle$ averaged over the flux distribution, are given. The most important contributions from the various neutrino flavors and neutrino parent types are shown.

Tab. 12 shows a summary on neutrino flux predictions, given in terms of total flux and mean neutrino energy averaged over the flux distributions, for the various neutrino flavors and for the most important neutrino parent types. The overall neutrino flux prediction is $5.22 \cdot 10^{-10}$ $cm^{-2}pot^{-1}$,

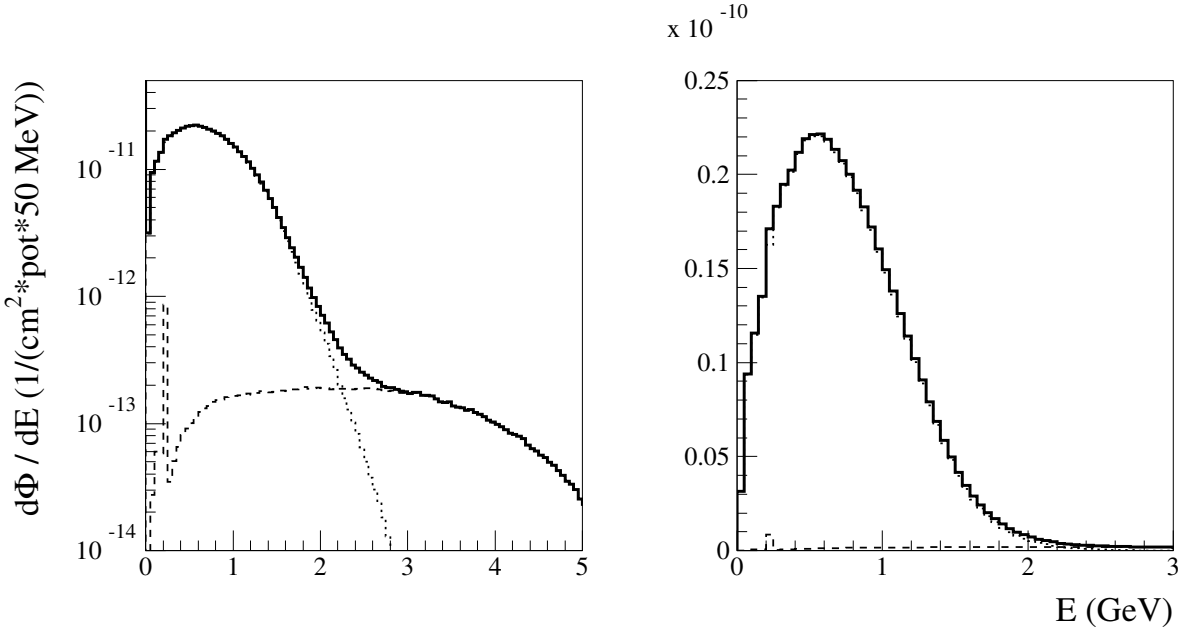

Figure 19: Predicted muon neutrino flux as a function of neutrino energy, for all muon neutrinos reaching MiniBooNE, in neutrino running mode. The solid histogram is for all muon neutrinos, the dashed histogram for muon neutrinos from K^+ decay, the dotted histogram for muon neutrinos from π^+ decay. The fluxes are shown on a logarithmic scale on the left, and on a linear scale on the right.

with a mean neutrino energy of 0.76 GeV. The flux prediction is $4.84 \cdot 10^{-10}$ $cm^{-2}pot^{-1}$ for muon neutrinos, $3.47 \cdot 10^{-11}$ $cm^{-2}pot^{-1}$ for muon antineutrinos, $3.07 \cdot 10^{-12}$ $cm^{-2}pot^{-1}$ for electron neutrinos, $3.44 \cdot 10^{-13}$ $cm^{-2}pot^{-1}$ for electron antineutrinos, yielding a 0.6% ν_e/ν_μ flux ratio, and a 0.7% $(\nu_e + \bar{\nu}_e)/(\nu_\mu + \bar{\nu}_\mu)$ flux ratio.

Figure 18 shows the neutrino energy distributions for muon neutrinos, muon antineutrinos, and electron neutrinos. Figure 19 shows the muon neutrino energy distribution, together with the partial contributions from π^+ and K^+ decays. Figure 20 shows the electron neutrino energy distribution, together with the partial contributions from μ^+, K^+, and K^0_L decays.

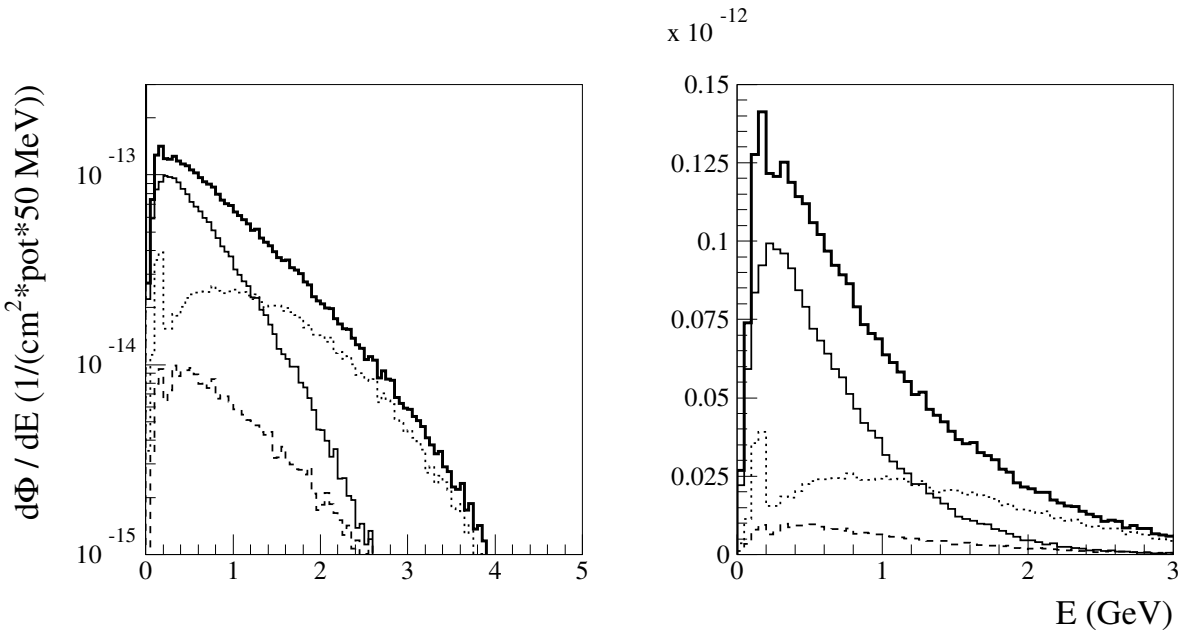

Figure 20: Predicted electron neutrino flux as a function of neutrino energy, for all electron neutrinos reaching MiniBooNE, in neutrino running mode. The thick solid histogram is for all electron neutrinos, the thin solid histogram for electron neutrinos from μ^+ decay, the dashed histogram for electron neutrinos from K^+ decay, the dotted histogram for electron neutrinos from K_L^0 decay. The fluxes are shown on a logarithmic scale on the left, and on a linear scale on the right.

9 Conclusions

In this technical note, the simulation programs currently used to predict the ν_e, $\bar{\nu}_e$, ν_μ, $\bar{\nu}_\mu$ fluxes at the MiniBooNE detector are described. The first simulation program is a GEANT4-based Monte Carlo code called `BooNEG4Beam`, and is responsible for simulating the chain of processes going from primary protons hitting the Beryllium target, until decays of mesons and muons yielding neutrinos occur. The second simulation program is a FORTRAN-based code called `BooBeamNT`, and is responsible for generating the neutrino kinematics distributions from meson and muon decays.

The most important design requirement is to provide a flexible and transparent physics interface to the user, in particular (but not only) concerning the physics of particle production in proton interactions in the MiniBooNE Beryllium target, because the uncertainties in the hadronic production models represent the dominant source of uncertainties in the MiniBooNE neutrino fluxes. The concrete implementation of this (and other) design requirement as a GEANT4 application is explained and motivated.

Over the past two and a half years, extensive validation of the code has been done, in conjunction with the code development. A number of cross-checks are presented in this note, aiming to quantify the accuracy of the simulation at the basic level of geometry specification, event generation, and description of the individual physics processes of relevance to MiniBooNE. A more complete (and complex) code validation has also been described, by comparing the `BooNEG4Beam` results to an independent simulation program, `Model_B`.

Finally, a summary on the ν_e, $\bar{\nu}_e$, ν_μ, $\bar{\nu}_\mu$ fluxes at the MiniBooNE detector, as predicted for the Dec04 baseline, is given.

10 Acknowledgments

I would like to thank Steve Brice, Daniel Elvira, Chris Green, Jeff Kallenbach, Geoff Mills, Byron Roe, Bill Seligman, Panagiotis Spentzouris, and Eric Zimmerman for useful suggestions on how to structure the code, and for building and maintaining the GEANT4 toolkit at FNAL. I would also like to thank Terry Hart, Peter Meyers, Geoff Mills, Jocelyn Monroe, Mike Shaevitz, and Sam Zeller for helping me in the code validation process. Finally, special thanks go to Dave Schmitz and Mike Wilking, who have brought very useful new functionalities into the GEANT4 code, and made this program a better simulation tool.

References

[1] M. Sung and H. White, "New Method for Neutrino Flux Measurement for BooNE", BooNE Technical Note # 88.

[2] S. H. Ahn *et al.* [K2K Collaboration], Phys. Lett. B **511**, 178 (2001) [arXiv:hep-ex/0103001].

[3] P. Astier *et al.* [NOMAD Collaboration], Phys. Lett. B **570**, 19 (2003) [arXiv:hep-ex/0306037].

[4] `http://wwwasd.web.cern.ch/wwwasd/geant4/G4UsersDocuments/Overview/html/`

[5] `http://www-boone.fnal.gov/software_and_analysis/beam_group/software/links/geant4/`

[6] B. Roe, "Some Thoughts on the Beam Monte Carlo", `http://www-boone.fnal.gov/memos/thoughts_on_MC.ps.gz`

[7] `http://www-boone.fnal.gov/software_and_analysis/boone-condor/`

[8] Y. Cho *et al.*, Phys. Rev. D **4**, 1967 (1971).

[9] J. Monroe, WIN2003 plot memos, "Sanford-Wang Fit to Pion Production Data", `http://www-boone.fnal.gov/memos/swfit.ps`

[10] `http://www-boone.fnal.gov/software_and_analysis/beam_group/`

[11] S. Eidelman *et al.* [Particle Data Group Collaboration], Phys. Lett. B **592**, 1 (2004).

[12] J, Monroe, "Comparison of MARS vs. GEANT3 Simulated Neutrino Flux in the MiniBooNE Detector Acceptance", BooNE Technical Note # 56

[13] V. V. Gachurin *et al.*, ITEP-59-1985

[14] Lykhachev, **ZETF 41** (1981) 39;

[15] Jon Link, private communication.

[16] Afonasiev, **YF 47** (1988) 1656.

[17] S. Geer, Phys. Rev. D **57**, 6989 (1998) [Erratum-ibid. D **59**, 039903 (1999)] [arXiv:hep-ph/9712290].

[18] L. M. Chounet, J. M. Gaillard and M. K. Gillard, Phys. Rept. **4**, 199 (1972).